Development of metakaolin-based geopolymer for selenium oxyanions uptake through in-situ ettringite formation

Xiaobo Niu [a], Yogarajah Elakneswaran [a *], Raudhatul Islam Chaerun [a], Chuwei Fang [a], Naoki Hiroyoshi [a], John L. Provis [b], Tsutomu Sato [a]

[a] Division of Sustainable Resources,

Graduate School of Engineering, Hokkaido University,

North 13, West 8, Sapporo, Hokkaido, Japan, 060-8628

[b] Department of Materials Science and Engineering,

The University of Sheffield, Sir Robert Hadfield Building,

Mappin St, Sheffield S1 3JD, The United Kingdom.

*Corresponding author

E-mail: elakneswaran@eng.hokudai.ac.jp

Tel: +81 11-706-7274

Abstract

Studies have demonstrated the remarkable capacity of metakaolin-based geopolymers for the uptake of cationic radionuclides, such as Cs^{+} and Sr^{2+}. However, the lack of uptake ability towards anionic radionuclides represents a potential avenue for improvement in utilising this material for nuclear waste disposal applications. Additionally, the prevalence of ettringite as an anion exchange agent formed in alkaline environments, such as cement hydration, is widely acknowledged in the field. However, no previous studies have been conducted to explore the utilisation of the advantageous qualities of both metakaolin-based geopolymer and ettringite in developing a comprehensive incorporation process for both cationic and anionic radionuclides. In this study, compositions and sets of preparation conditions were proposed to modify metakaolin-based geopolymer, resulting in the in-situ formation of ettringite, with the aim of enhancing its uptake capabilities for selenium oxyanions. The uptake behaviour and mechanism of ettringite, and geopolymer with in-situ ettringite, were proposed through co-precipitation experiments, binding and structural analysis. The results reveal that the ettringite can uptake SeO_3^{2-} and SeO_4^{2-} through co-precipitation; however, its effectiveness is limited to SeO_3^{2-} in the uptake process, where the mechanism is contingent on the concentration of Se oxyanions present. On the other hand, modified geopolymer with in-situ ettringite retained its capacity to uptake cationic radionuclides such as Cs^{+} and Sr^{2+} while evolving to exhibit an ability to uptake SeO_3^{2-}. Thermodynamic modelling was carried out according to the ion exchange mechanism, which effectively predicts the uptake of SeO_3^{2-} at low concentrations. The proposed composition and preparation conditions hold the potential for developing an effective incorporation process for cationic and anionic radionuclides. The outcomes of this research enhance the understanding of the uptake behaviour of Se oxyanions by ettringite and provide insight into the potential of metakaolin-based geopolymers to immobilise anions.

KEYWORDS:

Geopolymer; Ettringite; Uptake; Co-precipitation; Ion-exchange; Selenium oxyanions; Thermodynamic model

1. Introduction

Selenium (Se) is a widely occurring oxyanion-forming element. While it is considered a vital trace mineral in biological systems, it can pose a significant environmental and health hazard when its concentration surpasses certain levels. The aggregation of Se in high concentrations can be attributed to anthropogenic activities, and its cytotoxicity and carcinogenicity in animals have been demonstrated [1]. Among the various sources of Se aggregation, the nuclear industry is a particularly noteworthy contributor, as it has the potential to generate substantial amounts of the anionic radionuclide ^{79}Se. This isotope, ^{79}Se, is linked to fission, reprocessing, and accidents within the nuclear industry [2]. It is considered to be a high-priority radionuclide due to its long half-life of nearly 3.27×10^5 years and the presence of highly mobile oxidised forms, selenite (SeO_3^{2-}) and selenate (SeO_4^{2-}), which are regarded as particularly challenging species due to their high mobility in aqueous environments and severe toxicity [3,4]. Numerous techniques have been developed to mitigate the presence of selenium in wastewater effectively. Uptake methods utilising easily accessible sorbents, such as activated carbon, zeolites, resins, and iron-based materials, have demonstrated remarkable efficacy in removing selenium. These techniques have been successfully employed in the treatment of wastewater following the Fukushima Daiichi nuclear power plant accident [5,6,7,8,9]. In addition, emerging technologies such as membrane filtration [10], electrochemical processes [11,12], cationic layered rare earth hydroxide (LRHs) [13], tailored cationic polymeric [14], and cationic metal organic frameworks [15,16] have great potential for the effective immobilisation of many radioactive anions, including selenium oxyanions. However, it is crucial to acknowledge that these treatment approaches may lead to accumulating medium to high

concentrations of selenium aggregates, posing a potential risk of secondary contamination [17]. Hence, it is imperative to promptly develop encapsulate materials with low water solubility to ensure the formation of stable phases. Such materials can effectively immobilise selenium oxyanions and securely isolate selenium-bearing contaminants for long-term disposals, such as geological disposal [9].

Geopolymer materials (GP) are a well-known class of alkaline-activated materials. The geopolymerisation process can be succinctly described as the depolymerisation, polycondensation, and gel network formation of an aluminosilicate precursor in the presence of a strongly alkaline solution or activator [18,19]. As an alternative to Portland cement that is under assessment for nuclear waste management, the use of geopolymer has garnered interest worldwide [20]. Compared to conventional cementitious materials, the three-dimensional framework structure derived from oxygen-linked aluminium and silicon and the higher degree of silicate polymerisation, yield geopolymer materials with superior chemical durability [21,22].

The use of metakaolin-based geopolymers as a potential matrix for managing radionuclide-containing waste generated from the nuclear industry has received significant attention in recent years [23,24]. The nuclear industry is known to produce large quantities of contaminated wastewater containing radionuclides from various sources such as operation, maintenance, and accidents [2,25]. Extensive research has been conducted to explore the capabilities of metakaolin-based geopolymers as disordered pseudo-zeolite for the immobilisation of radionuclides. In their spatial structure, the tetrahedral aluminium sites possess a negative charge, which can be effectively neutralised by alkali cations derived from activator solutions [26]. These negative sites impart a permanent net negative framework charge to the metakaolin-based geopolymers, creating many sites capable of binding cations [27]. The uptake behaviour of metakaolin-based geopolymers for heavy metal ions has been confirmed and studied

92 extensively [28,29]. These geopolymers have also demonstrated remarkable efficiency in immobilising
93 ^{137}Cs and ^{90}Sr, the most prevalent cationic radionuclides found in water contaminated by nuclear
94 activities [30-33]. In our previous study [33], the mechanisms of ^{137}Cs, ^{90}Sr and ^{60}Co uptake by
95 metakaolin-based geopolymers were clarified, and a thermodynamic model based on ion exchange
96 mechanisms was proposed. However, the permanently negatively charged surface of metakaolin-based
97 geopolymers restricts the potential for uptake of anionic radionuclides such as selenium (^{79}Se) or iodine
98 (^{131}I). Hence, modifying the composition of metakaolin-based geopolymers to endow them with both
99 cations and anions uptake capacities while retaining their chemical stability remains a topic of great
100 interest in the field.
101
102 Ettringite ($3CaO{\cdot}Al_2O_3{\cdot}3CaSO_4{\cdot}32H_2O$) can be found as a naturally occurring mineral and is also one
103 of the hydration products of Portland cement. It predominantly forms during the initial stages of cement
104 hydration through the reaction between aluminate and sulphate, which can either be naturally present in
105 the cement paste or intentionally added to the system [34]. Ettringite possesses a column-like structure
106 wherein the $Al(OH)_6^{3-}$ octahedral units are interconnected with three adjacent Ca atoms. Each Ca atom
107 demonstrates square antiprismatic coordination, involving eight surrounding entities consisting of 4 H_2O
108 ($-OH_2$) molecules and 4 OH^- ions. Notably, the OH^- ions are shared between the $Al(OH)_6^{3-}$ octahedra
109 and the $Ca\text{-}O_8$ square antiprismatic polyhedra, facilitating their structural connectivity [35]. The column-
110 like structure is saturated with sulphate ions and water molecules, and these columns are held together
111 by the electrostatic attraction of the occupying species [36]. The abundant exchangeable sulphate (SO_4^{2-})
112 species in the inter-channels of its column-like structure endow ettringite with a remarkable capacity for
113 anion exchange [37,38]. For this reason, ettringite has been extensively studied for its ability to
114 immobilise selenium oxyanions. Solem-Tishmack et al. [39] found that ettringite derived from high-
115 calcium coal combustion by-products can effectively adsorb Se oxyanions from aqueous solutions.
116 Zhang et al. [40] reported that ettringite demonstrates a higher adsorption capacity for Se oxyanions than

117 does hydrocalumite, which represents another family of hydrous calcium aluminates that is often
118 observed among cement hydration products. Gou et al. found that ettringite can immobilise SeO_4^{2-}
119 through the formation of SeO_4^{2-} -substituted ettringite, while it can immobilise SeO_3^{2-} through a ligand
120 exchange with the Ca-OH_2 at the edges of its channels, forming an inner sphere complex [41,42].
121 Moreover, ettringite can form in environments that are alkaline and rich in calcium, aluminium, and
122 sulphur. Thus, it is feasible to form ettringite during aluminium-rich, alkali-activated reactions
123 (geopolymerisation) in the presence of calcium and sulphur-rich additives, such as slag [43,44], which
124 hold the potential for immobilising hazardous waste [45].
125
126 Several studies have examined ettringite formation in geopolymers made from multi-aluminosilicate
127 precursor sources [46,47]. Few researchers also explored the potential of geopolymers based on different
128 precursors to adsorb or immobilise anions, including I^-, AsO_4^{3-} and $Cr_2O_7^{2-}$ [48,49]. Tian et al. [50]
129 developed the uptake capability for Se oxyanions using layered double hydroxides (LDHs) based on
130 geopolymer gel. However, to our knowledge, the effectiveness of incorporating ettringite into
131 metakaolin-based geopolymers for the immobilisation of selenium oxyanions has not been reported and
132 studied in detail.
133
134 The present study addresses this gap by synthesising and evaluating a metakaolin-based geopolymer
135 with in-situ ettringite. The capacity and feasibility of ettringite to uptake Se oxyanions were evaluated
136 through aqueous co-precipitation experiments, and the uptake mechanism of the modified ettringite-in-
137 situ geopolymers was explored through a binding experiment. A combination of X-ray diffraction (XRD),
138 zeta potential, scanning electron microscopy (SEM), and Raman spectroscopy was used to evaluate the
139 solid-phase characteristics, while inductively coupled plasma mass spectrometry (ICP-MS) and ion
140 chromatography (IC) were used to analyse the aqueous phase. Finally, a thermodynamic model was
141 developed to understand selenite uptake in both synthetic ettringite and modified geopolymer with in-

142 situ ettringite. This comprehensive analysis provides valuable insights into the synthesis of ettringite-in-
143 situ metakaolin-based geopolymers and their ability to uptake Se oxyanions.
144

145 **2. Experimental**

146 **2.1. Materials**

147 Metakaolin obtained from Sobueclay (Japan), tricalcium aluminate (Taiheiyo Consultancy, Japan.
148 $3CaO{\cdot}Al_2O_3$, abbreviated as C_3A), gypsum (WAKO, 98 wt.%, $CaSO_4{\cdot}2H_2O$, abbreviated as Gyp), and
149 ground granulated blast furnace slag (Ceramento A, Taiheiyo Cement Sales Co., Ltd., Japan) were used
150 for the synthesis of geopolymer with in-situ ettringite. The chemical composition of metakaolin and slag
151 determined by X-ray fluorescence (XRF) is listed in **Table 1**. The calcium content (in the form of CaO)
152 in slag is approximately 0.01032 mol/g, and the molar ratio of SiO_2:Al_2O_3 of metakaolin is 1.01. An
153 aqueous potassium silicate solution (WAKO, originally containing 29.1 wt.% SiO_2, 21.9 wt.% K_2O, 49.0
154 wt.% H_2O), a potassium hydroxide (WAKO, 86 wt.% KOH), and ultrapure water (TRUSCO, Japan)
155 were used for making a potassium silicate alkali solution, which was used as an activator for the synthesis
156 of geopolymers. $Al_2(SO_4)_3{\cdot}16\text{-}18H_2O$ and $Ca(OH)_2$ were used to synthesise ettringite. In addition,
157 K_2SeO_3, K_2SeO_4 and $Sr(NO_3)_2$ were selected as the simulated radionuclide sources, purchased from
158 WAKO (Japan).
159

160 **Table 1.** Chemical composition (wt%) of the metakaolin and slag as determined by X-ray fluorescence

Component	Metakaolin	Slag
SiO_2	48.59	23.43
Al_2O_3	43.11	10.85
Fe_2O_3	0.54	0.50

CaO	0.21	51.70
MgO	3.66	4.11
Na_2O	2.25	2.54
K_2O	0.13	0.62
TiO_2	1.27	0.51
P_2O_5	1.08	1.23
SO3	-	4.00
L.O.I.*	1.74	2.40

*: L.O.I. is loss on ignition at 1100℃ for 12h [33,57].

2.2. Ettringite synthesis and co-precipitation

The process for the ettringite synthesis with and without Se oxyanions is shown in **Fig. 1 (a)**. Initially, 10 mmol/L $Al_2(SO_4)_3 \cdot 16\text{-}18H_2O$ and 60 mmol/L $Ca(OH)_2$ were mixed with water at a liquid/solid ratio of 10 to give a Ca^{2+} / SO_4^{2-} molar ratio of 2. The suspension was continuously magnetically stirred for 24 hours at room temperature, followed by vacuum filtration and then drying at 40 ℃ for one day. In addition, co-precipitation of ettringite in the presence of Se oxyanions was conducted. The raw materials for the ettringite formation of 10 mmol/L $Al_2(SO_4)_3 \cdot 16\text{-}18H_2O$ and 60 mmol/L $Ca(OH)_2$ were introduced into 100 mL K_2SeO_3 or K_2SeO_4 aqueous solution, where the concentration of Se oxyanions was from 0 to10 mmol/L. The synthetic geopolymer was added at a ratio of 1 g per 100 mL solution (**Fig.1(b)**), and they were subsequently mixed using a magnetic stirrer for 24 hours at room temperature. Then, the solid and liquid phases were separated by vacuum filtration for further analysis. All co-precipitation reactions were carried out in nitrogen-filled PE bottles to avoid CO_2 contamination. **Table 2** summarises the components included in each group. In addition, all solid samples were dried at 40 °C for 24 h in a thermostat before being ground to a particle size of less than 150 μm.

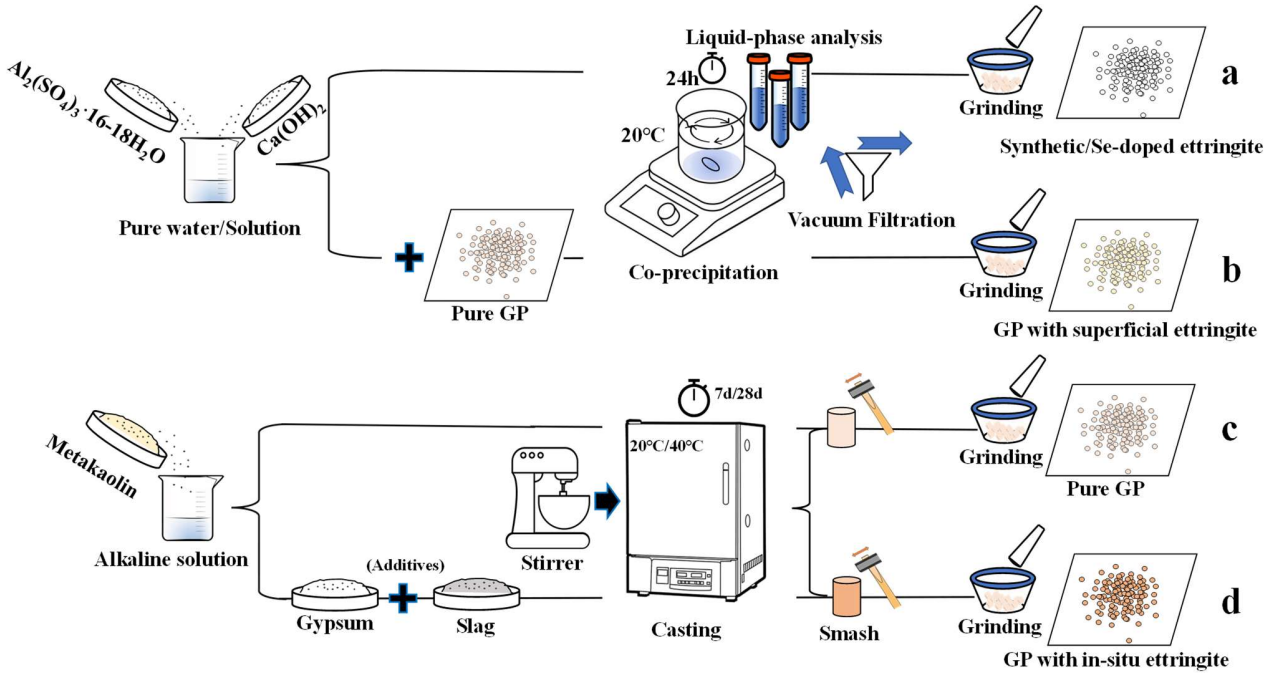

177

178 **Fig.1.** Schematic illustration of the procedure to conduct the co-precipitation experiment and to prepare
179 the samples of (a) synthetic/Se-doped ettringite, (b) geopolymer with superficial ettringite, (c) pure
180 geopolymers, and (d) geopolymers with in-situ ettringite

181

182 **Table 2.** Components contained in each group of co-precipitation experiment

Groups	SeO_3^{2-}	SeO_4^{2-}	Ettringite (raw material)	Geopolymer
1. SeO_4-Ettringite-GP		✓	✓	✓
2. SeO_4- Ettringite		✓	✓	
3. SeO_3- Ettringite -GP	✓		✓	✓
4. SeO_3- Ettringite	✓		✓	

183 ✓ indicates the presence of the component.

184 **2.3. Ettringite in-situ geopolymer synthesis**

185 The alkali-activated solution for synthesising the geopolymers samples was prepared from potassium
186 silicate solution, potassium hydroxide and ultrapure water. **Fig.1(c)** and **Fig.1(d)** demonstrate the
187 synthesis procedure of pure geopolymers and modified geopolymers with in-situ ettringite, respectively.
188 Pure geopolymers were prepared by mechanically mixing stoichiometric amounts of metakaolin with a
189 sufficient quantity of alkali-activated solution (**Fig.1(c)**), giving a final chemical composition of
190 geopolymers (in ceramist nomenclature) of $1K_2O$: $1Al_2O_3$:$1SiO_2$: $13H_2O$. The detailed synthesis
191 procedure, the preparation of materials and the curing method were reported in our previous study [33].
192 Various additives such as C_3A, Gyp and blast furnace slag with different doses and curing conditions
193 were tested to form the in-situ ettringite in geopolymer (**Table 3**). For simplicity, the samples were named
194 according to the additives and the content added to the system. For instance, Gyp 10 wt.% + 3Slag
195 corresponds to the sample synthesised by externally adding 10 wt.% gypsum and slag, the amount of
196 slag added was determined as the molar amount of calcium in the slag was three times the molar amount
197 of sulphate in added gypsum. After curing under specified conditions, the samples were characterised by
198 XRD to identify ettringite formation. The only group in which in-situ ettringite could be detected was
199 Gyp 10 w.t% + 3Slag, which had been kept at either 20 or 40 ℃ for 28 days.
200

201 **Table 3.** Compositions and conditions adopted for the formation of in-situ ettringite in geopolymer

Specimens with different additives	20℃ 7 days	20℃ 28 days	40℃ 7 days	40℃ 28 days
1. Synthetic ettringite				×
2. Ettringite raw materials: $Al_2(SO_4)_3 \cdot 16\text{-}18H_2O$ and $Ca(OH)_2$				×
3. C_3A 5 wt.% + Gyp 5 wt.%			×	×

4. C_3A 5 wt.% + Gyp 5 wt.% + 1Slag			×	×
5. C_3A 5 wt.% + Gyp 10 wt.%			×	×
6. C_3A 5 wt.% + Gyp 10 wt.% + 1Slag			×	×
7. C_3A 10 wt.% + Gyp 5 wt.%			×	×
8. C_3A 10 wt.% + Gyp 10 wt.%			×	×
9. Gyp 5 wt.%				×
10. Gyp 5 wt.% + 1Slag				×
11. Gyp 5 wt.% + 3Slag		×	×	×
12. Gyp 5 wt.% + 5Slag		×		×
13. Gyp 10 wt.%				×
14. Gyp 10 wt.% + 1Slag		×		×
15. Gyp 10 wt.% + 3Slag	×	✓	×	✓

×: No Ettringite was detected by XRD; ✓: Ettringite was detected by XRD

2.4. Experimental procedure

An X-ray diffractometer (MultiFlex, Rigaku, Japan) was used to characterise the synthetic samples with CuKα radiation, scanning from 2θ=5-45° with a scan speed of 6.5° per min and a step size of 0.02°. The microstructure of the geopolymer with in-situ ettringite was examined by scanning electron microscopy (SEM: JSM-IT200, JEOL, Japan) with a 25kV acceleration voltage. A zeta potential & particle size analyser apparatus (ELSZ-1000ZS) was used to measure the zeta potential of the suspensions where the solid/liquid ratio of the suspension was set to 1 g/L. In each case, KNO_3 was selected to adjust the ionic strength, whereas KOH was used to adjust the pH. The Raman spectra of the samples, including the structural variation of synthetic ettringite and geopolymer with in-situ ettringite after uptake of SeO_3^{2-}, were obtained using an XploRA PLUS Confocal Raman Microscope (HORIBA, Japan). The

experimental parameters applied were a laser power of 532 nm, an x50 VIS objective lens, a 50-100% filter, a 100 μm slit, a 300 μm hole, an 1800 grating (450-850 nm), a measurement time of 40 seconds, and 6 accumulations. The water content change in ettringite samples after uptake of SeO_3^{2-} was examined by a TG/DTA7220 (SEIKO, Japan), and the analysis was conducted by gradually increasing the temperature from 20 ℃ to 800 ℃ at a rate of 10 ℃/min while maintaining a nitrogen flow rate of 200 mL/min. The suspensions of ettringite were equilibrated with 0.01, 0.1, 1, and 10 mmol/L of K_2SeO_3 and K_2SeO_4 solutions to measure the equilibrium time for the uptake of ions by ettringite (1g synthetic ettringite powder per 100 mL solution). After 7, 14, 21 and 35 days of immersion, the solution was filtered using a syringe filter (0.45 μm), and the concentrations of Se oxyanions were assessed using inductively coupled plasma-mass spectrometry (ICP-MS, iCap Q ICP-MS, Thermo Scientific, USA, detection limit 0.01-10ppb), with the application of Yttrium internal standard method. A batch of binding experiments of synthetic ettringite and modified geopolymer with in-situ ettringite were performed with K_2SeO_3 solutions at 0.01, 0.05, 0.1, 0.5, 1, 5, and 10 mmol/L with an ettringite (in-situ ettringite) to solution ratio of 1g/100 mL. After equilibration, the liquid phase was filtered with a 0.45 μm syringe filter. The concentrations of Se oxyanions in the filtered solution were measured by ICP-MS, and the concentrations of SO_4^{2-} were measured through ion chromatography (ICS-90, DIONEX, USA). In addition, the uptake capacity of geopolymer with in-situ ettringite for Cs^+ and Sr^{2+} with in-situ ettringite was measured in the same way as given in our previous study [33]. It is important to note that a glovebox filled with N_2 gas and a sealed wide-mouth flask were employed in the experiment. Therefore, the influence of oxygen was negligible. In addition, the redox state regions expressed by Eh-pH according to the boundary conditions set in terms of pH and initial concentration of SeO_3^{2-} are shown in **Fig. S1**. The result illustrates that all the data points fall within the range dominated by SeO_3^{2-}. Hence, the oxidation of SeO_3^{2-} to SeO_4^{2-} in this study was found to be insignificant. Furthermore, it is known that SeO_4^{2-} represents the highest oxidation state of selenium and is considerably more stable compared to SeO_3^{2-}, and it will rarely be actively reduced to SeO_3^{2-} in the absence of a suitable reducing agent [51].

Given this understanding, it can be inferred that throughout this study, SeO_3^{2-} and SeO_4^{2-} retained their respective oxidation states without undergoing any notable redox reactions.

The amounts of bound Se oxyanions and leached SO_4^{2-} were calculated by Eqs. (1) and (2):

$$A_B = \left(C_{Se\_i} - C_{Se}\right)\frac{V}{m}\ (mmol/g) \quad (1)$$

$$A_L = \left(C_S - C_{S\_b}\right)\frac{V}{m}\ (mmol/g) \quad (2)$$

The distribution ratio (R_d) was determined from Eq. (3):

$$R_d = A_B / C_{Se\_i}\ (L/g) \quad (3)$$

where A_B is the bound amount of the Se (mmol/g), A_L is the leached amount of SO_4^{2-} (mmol/g), C_{Se_i} is the Se initial concentration (mmol/L), C_{Se} is the equilibrium concentration of the Se (mmol/L), C_S is the equilibrium concentration of SO_4^{2-} (mmol/L), and C_{S_b} is the SO_4^{2-} concentration when the synthetic ettringite or geopolymer with in-situ ettringite is immersed in pure water until reaching equilibrium (mmol/L). V is the volume of the liquid phase (L), and m is the mass (g) of the crystalline ettringite detected by XRD.

2.5. Modelling approach

The ion-exchange reaction between synthetic ettringite or in-situ ettringite and SeO_3^{2-} was fitted and explained based on the ion-exchange model available in the geochemical code PHREEQC Version 3 [52]. The activity coefficients were calculated based on the extended Debye–Huckel equation, whose parameters are available in the database of WATEQ4F.dat [53]. The simulant radionuclide anion SeO_3^{2-} can be exchanged with the SO_4^{2-} present in the ettringite interlayers as

$$Xg - SO_4 + {SeO_3}^{2-} \leftrightarrow Xg - SeO_3 + {SO_4}^{2-}, K = \frac{[Xg-Se_{\ 3}][{SO_4}^{2-}]}{[Xg-SO_4][{SeO_3}^{2-}]} \quad (4)$$

where Xg is the exchange site, simplifying the representation of the ettringite interlayer. K is the exchange coefficient for SeO_3^{2-}. The model can be implemented in PHREEQC using the keyword data block of EXCHANGE_MASTER_SPECIES, EXCHANGE_SPECIES, and EXCHANGE. In addition, the keyword data block of PHASES and EQUILIBRIUM_PHASES was used to introduce the ettringite phase into the reaction to simulate the pH changes and the SO_4^{2-} environment in the solution through the equilibrium reactions. To obtain the best-fitting $\log\_K$, a Python code loop was implemented to adjust the parameter continuously in incremental steps. This iterative process involved comparing the quality of the fit controlled by $\log\_K$ with the experimental data until the desired level of accuracy was achieved. Python-IPhreeqcCOM code for the ion exchange model is given in the Supporting Information.

3. Results and discussion

3.1 Characterisation

X-ray diffraction measurements were conducted to characterise the formation of in-situ ettringite in modified geopolymers. **Fig. 2** shows the XRD patterns of pure geopolymer, synthetic ettringite, and geopolymer with in-situ ettringite cured at 20 ℃ and 40 ℃ for 28 days. A small amount of gypsum was found as an impurity in the synthetic ettringite, less than 2 %, as determined using a corundum internal standard. The synthetic geopolymer XRD pattern exhibits a broad hump in the range of 2θ = 27°-29°, indicating disordered products. A faint signal of quartz was also detected in the XRD pattern of pure geopolymer, attributed to a very minor impurity in the metakaolin used. These findings align with earlier investigations on metakaolin-based geopolymers [33]. The characteristic peaks of ettringite were detected in the XRD pattern of the geopolymer samples with in-situ ettringite; however, the presence of

peaks of potassium sulphate was also identified, which could be a result of the precipitation of saturated sulphate with potassium ions in the pore solution of the geopolymer. It is believed that the presence of the sulphate ions would favour the formation of in-situ ettringite, although there may be some delay in this process [54]. The sample containing Gyp 10 wt.% + 3Slag-40°C exhibited a significantly stronger ettringite peak, measuring 2.65% according to the internal standard method. A calcite peak was also observed in this sample, unlike in the Gyp 10 wt.% + 3Slag-20°C sample. These findings indicate that a relatively higher temperature favours the crystallisation of these crystals and that the higher temperature used here is sufficiently low not to induce thermal destabilisation of the ettringite.

Fig. 3 shows the SEM images of pure geopolymers, synthetic ettringite and the Gyp 10 wt.% + 3Slag-40°C samples. These images provide insights into the significant morphological changes in geopolymers before and after in-situ ettringite formation. An amorphous geopolymer matrix is shown in **Fig. 3 (a)**; the EDS analysis indicates that its main constituent elements are O, Al, and Si in the structural and K is balancing the negative charge sites. The characteristic needle-like hexagonal crystal structure of ettringite is clearly depicted in **Fig. 3 (b)**. Notably, the EDS analysis reveals a slight elevation of approximately 3.5% in the S and Ca as compared to the anticipated theoretical values. This discrepancy can likely be attributed to the presence of $CaSO_4$ impurities, which may have influenced the detection results. Moving on to the modified geopolymers shown in **Fig. 3 (c)**, the presence of in-situ ettringite embedded within the geopolymer matrix is evident. The EDS analysis performed at specific points confirms the corresponding elemental composition of the substances. Although Ca was detected in the geopolymer matrix and Si in the in-situ ettringite, this occurrence might be attributed to their interaction during the detection process. Significantly, the in-situ ettringite within the geopolymer matrix is not observed in aggregated clusters, as typically observed in cementitious materials [55]. Instead, it appears as a distinct crystal structure embedded within the geopolymer matrix. This phenomenon is likely a consequence of the electrostatic attraction between the positive charge on the ettringite surface and the geopolymer

matrix's negative charge. This electrostatic interaction is further addressed in the subsequent sections of this paper, specifically in the discussion on zeta potential. It is therefore hypothesised that the in-situ ettringite present in the geopolymer matrix may have distinct properties compared to synthetic ettringite.

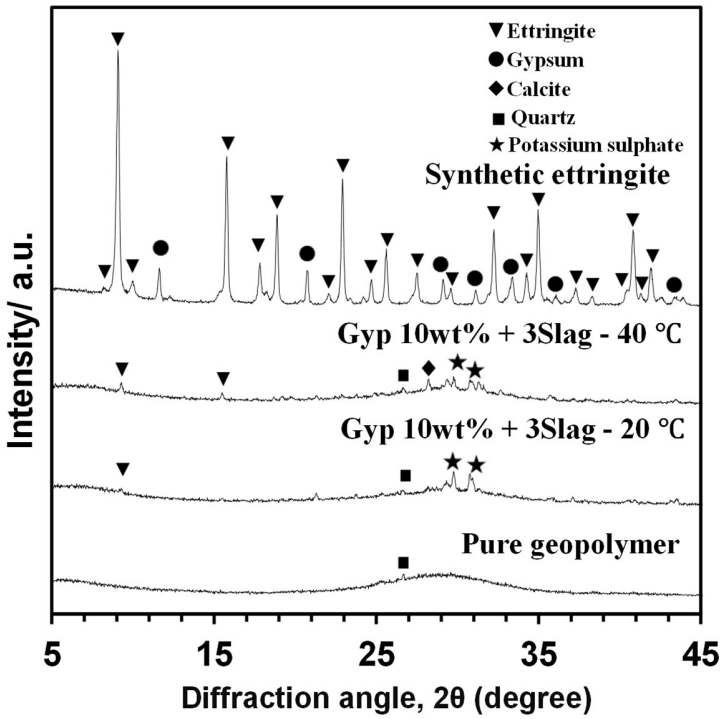

Fig. 2. X-ray diffraction (XRD) patterns of synthetic ettringite, pure and modified geopolymers.

316

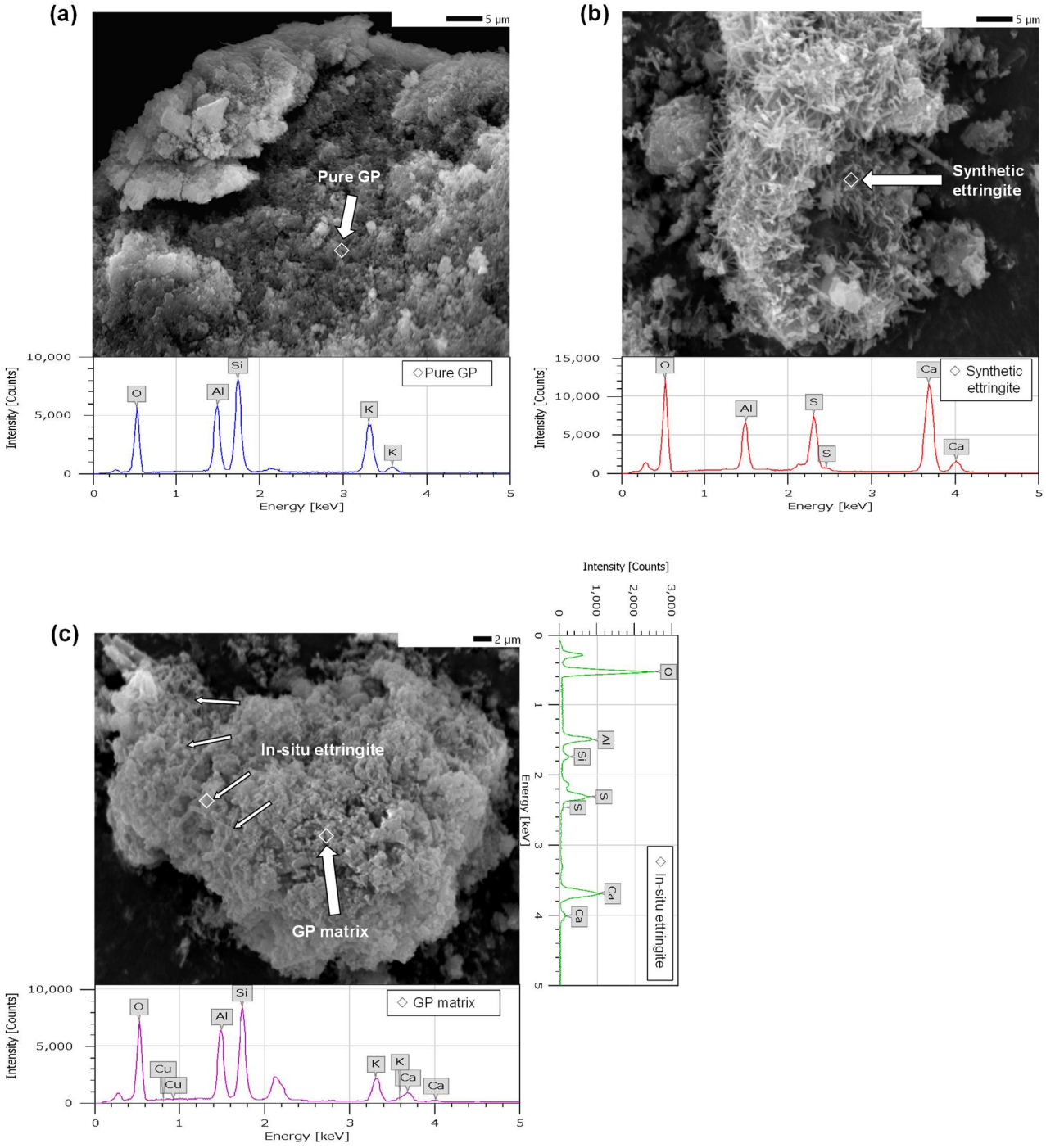

317

318 **Fig. 3.** SEM micrographs of (a) pure geopolymer, (b) synthetic ettringite and (c) modified geopolymer

319 and EDS analysis of the corresponding sites

320

The zeta potential of each solid phase is demonstrated in **Fig. 4**. Since those solid phases were in an alkali-activated environment, basic solutions were selected for zeta potential measurement at constant ionic strengths of 10 and 100 mmol/L. Synthetic ettringite shows a positive zeta potential that is independent of pH, indicating the presence of a permanent charge on its surface (**Fig. 4 (a)**). The positive charges are considered to be derived from the unit cell of ettringite consisting of columnar $\{Ca_6[Al(OH)_6]_2 \cdot 24H_2O\}^{6+}$ [35]. Conversely, the zeta potential of pure geopolymer shows a consistent negative charge independent of pH (**Fig. 4 (b)**). However, as the ionic strength decreased, a thicker electrical double layer formed, increasing the absolute magnitude of the zeta potential of the pure geopolymer. It is worth noting that the zeta potential of ettringite was independent of ionic strength, which could be a significant characteristic difference in its behaviour compared to the zeta potential of geopolymer. Both the geopolymer with superficial ettringite from the co-precipitation process and the geopolymer with in-situ ettringite after modification demonstrated a reduced absolute value of zeta potential due to the positive surface of ettringite partially compensating the negatively charged geopolymer matrix (**Fig. 4 (c) & (d)**). Moreover, due to the variation in the state of the space filled by ettringite, the zeta potential of the geopolymer with superficial ettringite exhibited a trend more like that of ettringite, while the surface of geopolymer with in-situ ettringite behaved similarly to pure geopolymer.

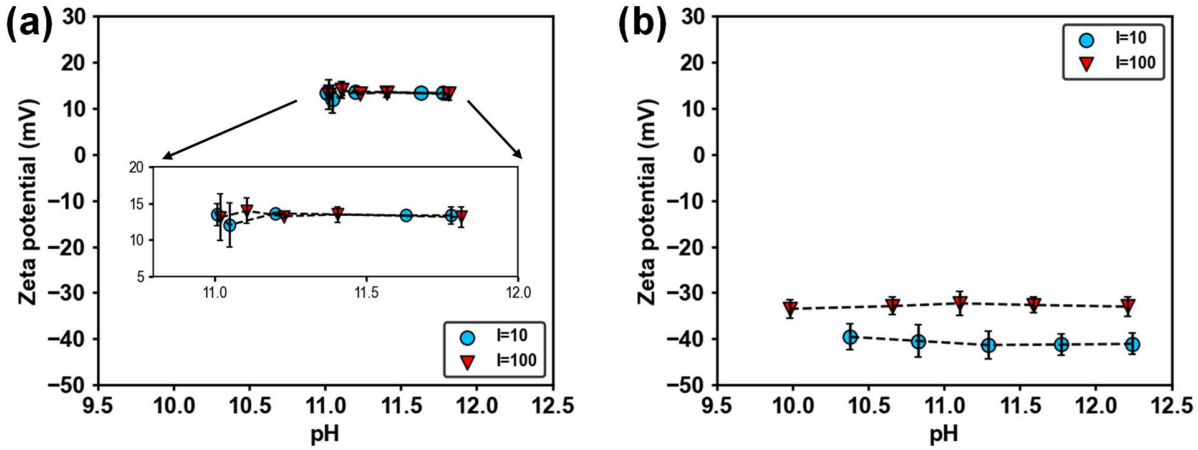

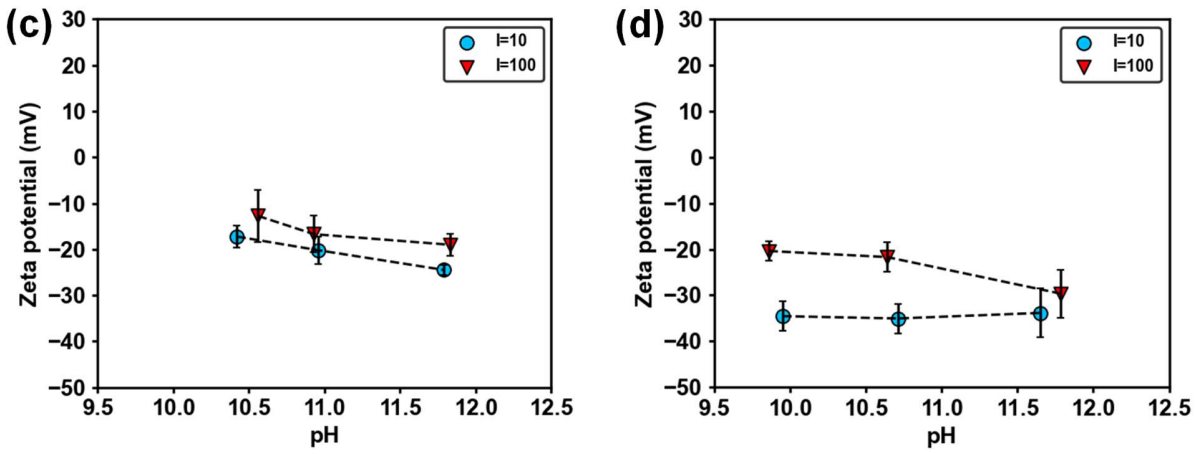

Fig. 4. Zeta potential as a function of pH for (a) synthetic ettringite, (b) pure geopolymer, (c) geopolymer with superficial ettringite and (d) geopolymer with in-situ ettringite (legend entries indicate ionic strengths of 10 and 100 mmol/L)

The synthetic ettringite was characterised by Raman spectroscopy (**Fig. 5 (a)**). The peak at 989, 450, 1118 and 615 cm^{-1} are (respectively) the v_1, v_2, v_3 and v_4 sulphate anion vibration modes and the peak at 549 cm^{-1} is due to the bending vibration mode of $Al(OH)_6$ [56]. In addition, the Raman spectroscopic analysis of pure geopolymer and geopolymer with in-situ ettringite indicates the change of structure and components after modification (**Fig. 5 (b)** and **Fig. 5 (c)**). Previous studies have reported that the most sensitive and typical bands of geopolymer structure in Raman spectroscopy were in the range of 350-750 cm^{-1} [57]. The peaks at 395(396), 509(507) and 635 cm^{-1} are assigned to the vibration modes of the representative ring structures of aluminosilicate tetrahedra in geopolymers. The broadband at 372-421 cm^{-1} (marked as light blue in **Fig. 5**) is assigned to 8-membered rings (8R), the broadband in the region of 421-604 cm^{-1} (marked as light green) representing double 6-membered rings (D6R), and the broadband at 604-712 cm^{-1} (marked as light red) corresponding to 4-membered rings (4R). These are the main basic building units that constitute the three-dimensional network of the geopolymer, which is a disordered pseudo-zeolite [58]. It is important to note that the 8R, D6R, and 4R vibration modes of the modified

geopolymer containing in-situ ettringite remained unaltered from the pure geopolymer (**Fig. 5 (b)** and **Fig. 5 (c)**); intensities and frequencies were nearly constant, indicating that the geopolymer matrix was not structurally altered by the addition of slag and gypsum to form in-situ ettringite. No new chemical linkages were observed that would have suggested a chemical connection between the geopolymer matrix and the ettringite. Additionally, the sample containing in-situ ettringite shows a minor calcium carbonate impurity due to adding calcium (as slag and gypsum) into the geopolymer (**Fig. 5 (c)**).

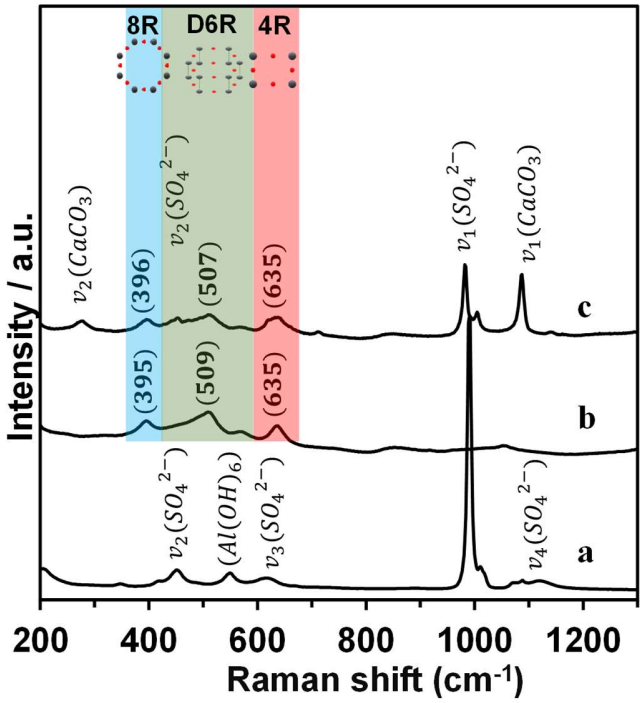

Fig. 5. Raman spectra of (a) synthetic ettringite, (b) pure geopolymer, and (c) modified geopolymer with in-situ ettringite

3.2 Co-precipitation analysis

The equilibrated Se oxyanions and sulphate concentration of co-precipitation groups 1-4 (as defined in **Table 2**) are shown in **Fig. 6**. As the initial Se concentration increased, the removal of both SeO_3^{2-} and SeO_4^{2-} from the solution grew, and the difference between each group became more pronounced (**Fig. 6 (a)**). According to previous studies [42, 59], ettringite has been shown to immobilise SeO_3^{2-} more

372 effectively than SeO_4^{2-}, resulting in the formation of Se-doped ettringite, and the results presented here
373 are broadly consistent with that past studies. The addition of geopolymer reduces the Se removal due to
374 the charge repulsion caused by the negatively charged surface of the geopolymer (**Fig. 4**). As the amount
375 of immobilised Se increased (**Fig. 6 (a)**), the concentration of sulphate (SO_4^{2-}) in the solution also rose
376 correspondingly (**Fig. 6 (b)**). This results from replacing sulphate as the free anion within the ettringite
377 columnar structure by the Se oxyanions. Given that the original sulphate concentration was 30 mmol/L,
378 the decrease in sulphate can be interpreted as an indication of the extent of ettringite formation. It is
379 found that the presence of geopolymer hindered the formation of ettringite in a co-precipitation system
380 to some extent.
381
382 Comparing the deviation in equilibrated concentrations of each species with the blank group (without
383 Se) is crucial for understanding the uptake of ettringite during the co-precipitation process with Se
384 oxyanions. The difference between the initial and equilibrated Se concentration for groups 1-4 at 10
385 mmol/L Se initial concentration (**Fig. 6 (a)**), which could be regarded as the amount of Se taken up by
386 the solid, were 1.81, 2.17, 6.94 and 9.36 mmol/L, respectively. Correspondingly, the differences in
387 sulphate concentration between the blank and the equilibrated samples were 1.59, 2.16, 6.3 and 7.24
388 mmol/L, respectively (**Fig. 6 (b)**), which could be regarded as the amount of SO_4^{2-} displaced from
389 ettringite. A very close relationship was thus found between the uptake amount of Se oxyanions and the
390 displaced amount of SO_4^{2-} in groups 1, 2, and 3, but there is a significant difference in group 4. It is
391 believed that SeO_4^{2-} and SeO_3^{2-} uptake in groups 1-3 was primarily facilitated by the formation of Se-
392 doped ettringite, in which Se oxyanions were immobilised as interlayer anions through electrostatic
393 forces. However, the immobilisation of Se in group 4 is not solely attributed to anion exchange with
394 inter-column sulphate, suggesting another mechanism appears to play a role. A previous research study
395 [42] suggested that ligand exchange with the $-OH_2$ groups at the channel edges to form complexes could
396 be one of the dominant mechanisms for SeO_3^{2-} uptake in ettringite, and it is possible that this is taking

place in group 4. This mechanism will be discussed in more detail in the following section. The results of R_d with an increasing initial concentration of Se are shown in **Fig. 6 (c)**. The R_d of ettringite for SeO_3^{2-} is much higher than that of SeO_4^{2-} and gradually decreases with an increasing initial concentration of Se. Despite the slight decrease in R_d for SeO_4^{2-} with higher initial Se concentration, this decrease is relatively insignificant compared to the significant alterations observed in the SeO_3^{2-} system. It can be observed that despite some negative effects of the presence of geopolymer on the immobilisation of Se oxyanions, ettringite still exhibits a significant ability to immobilise Se oxyanions.

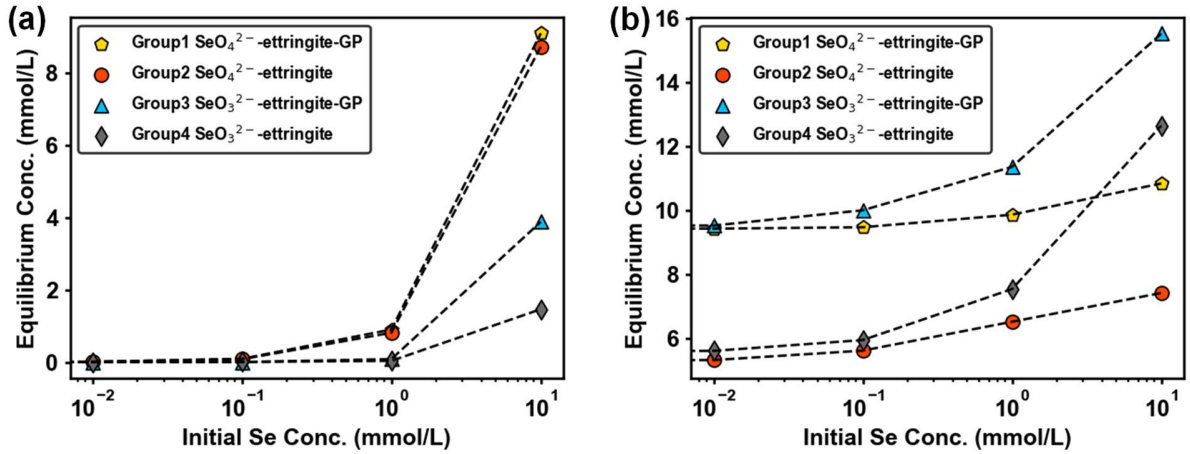

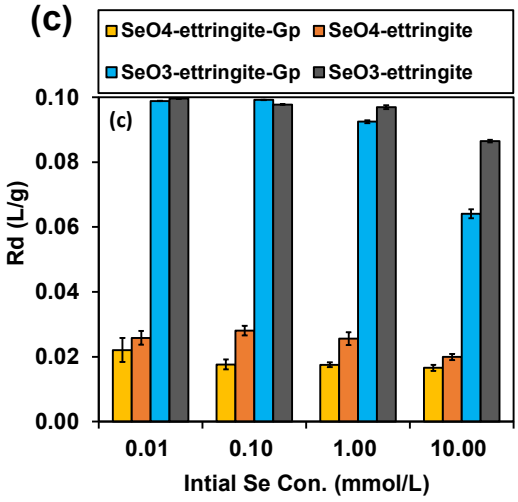

Fig. 6. Concentration of (a) Se oxyanions, (b) SO_4^{2-} at equilibrium, and (c) calculated distribution ratio (R_d) as a function of initial Se concentration (The pH range of systems with only ettringite was 10.5±0.1, and the pH range of systems with geopolymer was 11±0.1)

The XRD patterns of the solid phases resulting from the co-precipitation systems were analysed, and the interplanar distance at (100) crystal planes, d_{100}, was obtained by applying the Bragg formula to the 2θ angle of the (100)-plane peak. **Table 4** presents the d_{100} values for synthetic ettringite, serving as a control, and the d_{100} values of Se-doped ettringite equilibrated in a system containing an initial concentration of 10 mmol/L Se. The d_{100} of ettringite in the control group had no significant difference in the presence or absence of geopolymer. After the uptake of SeO_4^{2-} and SeO_3^{2-}, the d_{100} of ettringite increased and decreased, respectively. The state of the intercolumn free water has no impact on the size of a unit cell or crystal structure [60]; thus, the variation of the interplanar distance can be attributed to the uptake of Se oxyanions. The replacement of SO_4^{2-} by the Se oxyanions appears to increase in the interplanar distance due to the larger size of SeO_3^{2-} and SeO_4^{2-}, as the Se-O bond length is longer than the S-O bond length [61]. However, the uptake of SeO_3^{2-} did not increase d_{100}; the difference between the uptake behaviour of ettringite toward SeO_3^{2-} and SeO_4^{2-} can be attributed to the structural distinction between the two species [42, 62, 63].

Notably, the presence of geopolymer may impact the change in d_{100} of ettringite after the uptake of SeO_3^{2-} while having a relatively small impact on the change in d_{100} after the uptake of SeO_4^{2-}. This outcome suggests that geopolymer may impede the formation of complexes through ligand exchange, but the capacity of ettringite to immobilise Se oxyanions through interlayer electrical attraction is not significantly affected. In addition, it is essential to note that the d_{100} value of synthetic ettringite is influenced by various factors, such as the Ca/Al ratio, differences in crystallinity resulting from the growth environment of the crystals, and changes in orientation caused by cutting and grinding during

sample preparation. Previous studies have reported d_{100} values of ettringite ranging from 9.67 to 9.75 Å [35, 64-66]. Therefore, the d_{100} value obtained for the synthetic ettringite in this study is considered to be within a reasonable range.

Table 4. The shift in the d_{100}-spacing of ettringite at a concentration of 10 mmol/L Se in each group and the percentage change compared to synthetic ettringite

	d_{100}, ettringite control sample (Å)	d_{100}, ettringite equilibrated at 10 mmol/L Se (Å)	d_{100}, change after uptake Se (10mmol/L) (%)
1. SeO_4- ettringite -GP	9.733 ± 0.01	9.815	+ 0.842
2. SeO_4- ettringite		9.812	+ 0.812
3. SeO_3- ettringite -GP		9.697	- 0.369
4. SeO_3- ettringite		9.676	- 0.586

3.3 Uptake behaviour from solution

Prior to determining the Se oxyanion uptake from the solution onto the synthetic ettringite and the geopolymer with in-situ ettringite, the time required to attain equilibrium was determined. **Fig. 7** presents the R_d values of SeO_3^{2-} and SeO_4^{2-} on synthetic ettringite as a function of time in solutions with concentrations ranging from 0.1 to 10 mmol/L. The R_d of SeO_3^{2-} attained more than 95% of its highest value after 7 days and more than 99% of its highest value after 14 days. Similar trends were observed across all concentrations. As such, 14 days is considered as the equilibration time for the isothermal uptake experiment. On the other hand, little SeO_4^{2-} could be immobilised even after 35 days of immersion, which indicates ettringite has a limited capacity to immobilise SeO_4^{2-} from solution (as distinct from the co-precipitation route discussed in the previous section). Therefore, the primary emphasis of the

449 isothermal uptake in this study is on SeO_3^{2-} uptake by geopolymers with in-situ ettringite and by the
450 synthetic ettringite.

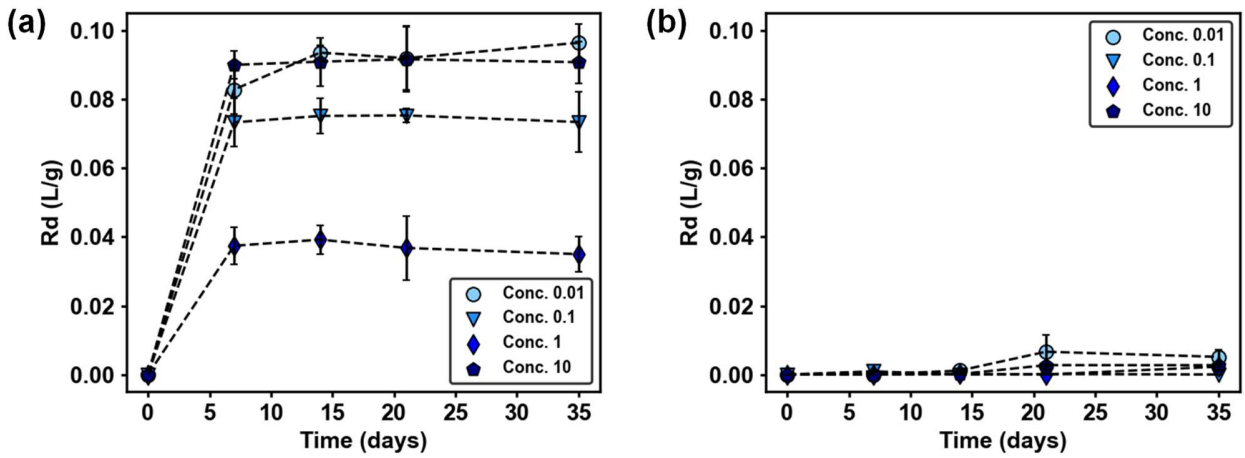

451

452 **Fig. 7.** Relationship between distribution ratio (R_d) and immersion time for synthetic ettringite in (a)
453 SeO_3^{2-} and (b) SeO_4^{2-} solutions of different concentrations (marked in the legends, in units of mmol/L,
454 and the pH range of all concentration systems was 10.5±0.1)

455

456 The relationship between the quantity of leached SO_4^{2-} ions from synthetic ettringite and from the
457 modified geopolymer with in-situ ettringite and the amount of bound SeO_3^{2-} ions is presented in **Fig. 8**.
458 The relationship between leached SO_4^{2-} and bound SeO_3^{2-} at initial SeO_3^{2-} concentrations below 1
459 mmol/L displays a direct (1:1) linear correlation onto both synthetic ettringite and geopolymer with in-
460 situ ettringite. However, at high SeO_3^{2-} concentrations (5 and 10 mmol/L), both geopolymer with in-situ
461 ettringite and synthetic ettringite exhibit correlations that deviate somewhat from the expected direct
462 linear relationship. In particular, there is a slight deviation for geopolymer with in-situ ettringite and a
463 significant deviation for synthetic ettringite. This suggests that the amount of bound SeO_3^{2-} exceeded that
464 of released SO_4^{2-}. Based on a previous study [67], the quantity of SO_4^{2-} available for ion exchange in the
465 ettringite is estimated to be 0.04 mmol SO_4^{2-} per gram of ettringite, representing approximately 2-3% of
466 the total sulphate present in the solid. The results of the current study indicate that the experimental

uptake of SeO_3^{2-} and leaching of SO_4^{2-} at an initial SeO_3^{2-} concentration of 1 mmol/L (considered the maximum concentration for ion exchange) were approximately 0.037 mmol/g and 0.036 mmol/g, respectively. These findings are in good agreement with the estimated results and support the mechanism of ion exchange.

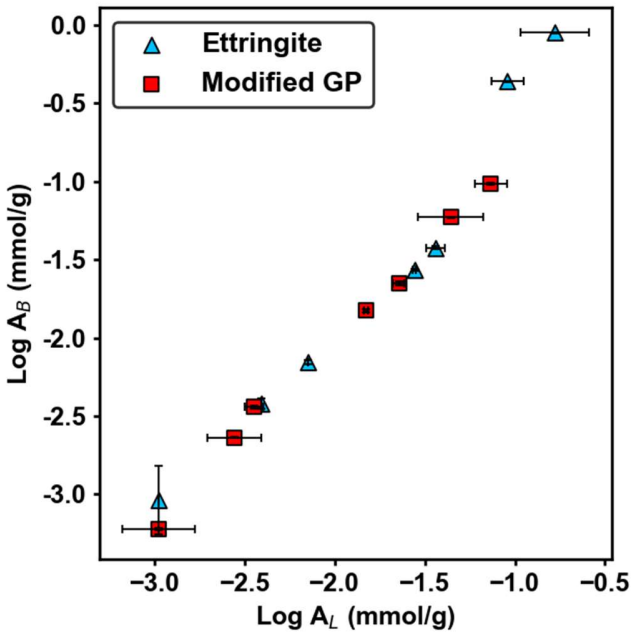

Fig. 8. The relationship between bound SeO_3^{2-} and released SO_4^{2-} from synthetic ettringite (blue triangle) and geopolymer with in-situ ettringite (red squares), expressed in mmol of the oxyanions per g solids (The pH range of systems with ettringite was 10.5±0.1, and the pH range of systems with modified geopolymer was 11.5±0.2)

Fig. 9 displays the evaluation of R_d and the leaching/binding ratio (L/B) as a function of increasing initial SeO_3^{2-} concentration. The L/B ratio represents the molar ratio between the amount of leached SO_4^{2-} and the amount of bound SeO_3^{2-}. The R_d of geopolymer with in-situ ettringite continuously decreased with increasing SeO_3^{2-} initial concentration, whereas the L/B ratio remained close to 1 for concentrations below 1 mmol/L and showed a slight decline for concentrations greater than 1 mmol/L. Although the L/B ratio significantly deviated from 1 at 0.01 mmol/L, possibly due to measurement uncertainty. As

opposed to that, the R_d of synthetic ettringite showed a "U"-shaped relationship with different initial SeO_3^{2-} concentrations: in the concentration range from 0.01 to 1 mmol/L, the R_d of synthetic ettringite decreased with increasing initial SeO_3^{2-} concentration similar to the geopolymer with in-situ ettringite, while the R_d sharply increased when the concentration was elevated to around 5 mmol/L, (approaching the same high R_d as at 0.01 mmol/L), and it then remained constant up to 10 mmol/L initial concentration. The L/B ratio of SeO_3^{2-} on synthetic ettringite fluctuated around 1 in the concentration range between 0.01 and 1 mmol/L SeO_3^{2-} but rapidly decreased when the initial SeO_3^{2-} concentration reached 5 mmol/L. These fluctuations suggest that the SeO_3^{2-} uptake in ettringite, both synthetic form and in-situ form, is primarily controlled by anion exchange with SO_4^{2-} from the interlayer at concentrations below 1 mmol/L. When the concentration of SeO_3^{2-} exceeds 1 mmol/L, the uptake mechanism for SeO_3^{2-} shifts to ligand exchange, which acts in conjunction with ion exchange. However, this mechanism is considerably impeded in the in-situ form of ettringite.

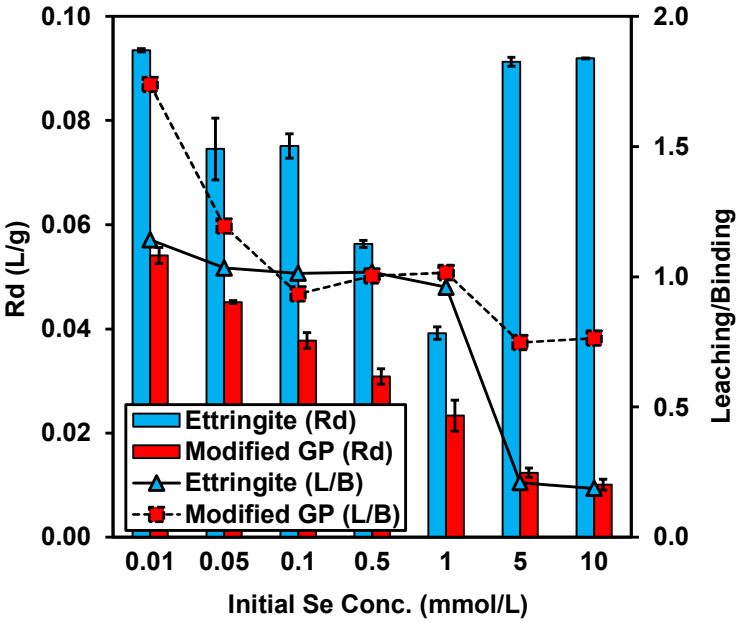

Fig. 9. R_d values and leaching/binding (L/B) ratios of SeO_3^{2-} on synthetic ettringite, and on geopolymer with in-situ ettringite, as a function of initial SeO_3^{2-} concentration (The pH range of systems with ettringite was 10.5±0.1, and the pH range of systems with modified geopolymer was 11.5±0.2)

499 The Cs^+ and Sr^{2+} uptake capacities of pure geopolymer and geopolymer with in-situ ettringite were also
500 analysed and compared, as depicted in **Fig. 10**. It was observed that the capacity of pure geopolymer for
501 both Cs^+ and Sr^{2+} was consistently higher than that of the geopolymer with in-situ ettringite, with a more
502 significant difference in capacity towards Sr^{2+} as compared to Cs^+. While both pure geopolymer and
503 geopolymer with in-situ ettringite exhibited an increase in cation uptake with increasing initial cationic
504 concentration until a concentration of 5 mmol/L, the pure geopolymer continued to uptake more cations
505 even when the initial concentration exceeded 5 mmol/L. However, the uptake capacity of geopolymer
506 with in-situ ettringite appeared to reach saturation at around 5 mmol/L, unable to continuously uptake
507 more cations. This disparity can be attributed to the positive surface charge of the in-situ ettringite, which
508 reduces the electrostatic attraction and leads to a partial loss of chemical sites available for cation
509 exchange. However, it is important to note that the actual concentrations of cations like Cs^+ and Sr^{2+} in
510 pollutants are in the order of parts per million, thus even with the modification, geopolymer with in-situ
511 ettringite still possesses a beneficial uptake capacity for Cs^+ and Sr^{2+}.

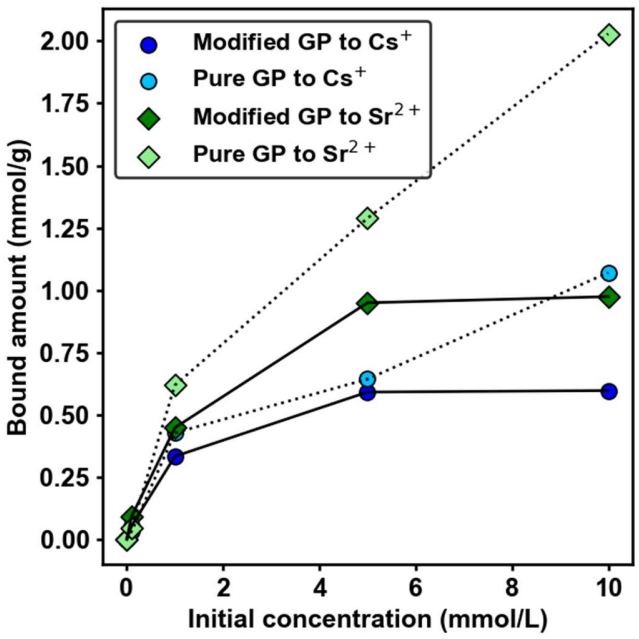

512

513 **Fig. 10.** Uptake capacity of pure geopolymer (dotted lines) and geopolymer with in-situ ettringite (solid
514 line) for Cs^+ and Sr^{2+}

3.4 Structural change after uptake

The structural changes in synthetic ettringite, and geopolymer with in-situ ettringite, after SeO_3^{2-} uptake can be characterised using Raman spectra, as shown in **Fig. 11**. The spectra in **Fig. 11(a)** depict the Raman spectra of synthetic ettringite before and after 14 days of immersion in solutions with varying SeO_3^{2-} initial concentrations. As previously discussed (**Fig. 5**), the peaks at 989, 450, 615, and 1118 cm^{-1} correspond to the vibrations of SO_4^{2-}, while the peak at 549 cm^{-1} is due to the bending vibration mode of $Al(OH)_6$. These peaks remained stable after 14 days of immersion and showed no significant changes with initial SeO_3^{2-} concentration changes. The broad band between approximately 3000 cm^{-1} to 3650 cm^{-1} is caused by the overlapping bands of channel water, crystal water, and coordinated -OH_2 vibrations in the columnar unit of ettringite. Synthetic ettringite and ettringite immersed in solutions with initial SeO_3^{2-} concentrations ranging from 0 to 0.5 mmol/L exhibited identical spectra in the 3000 cm^{-1} to 3650 cm^{-1} range, but the intensity in this region decreased gradually with increasing initial SeO_3^{2-} concentration, reaching a significant reduction when the initial SeO_3^{2-} concentration reached 10 mmol/L. It is also worth mentioning that with increasing initial SeO_3^{2-} concentration, new peaks attributed to SeO_3^{2-} became gradually revealed at 829 cm^{-1} and 773 cm^{-1}.

Fig. 11 (b) shows the Raman spectra of the geopolymer with in-situ ettringite after 14 days of immersion. A comparison between the pure geopolymer and the geopolymer with in-situ ettringite demonstrates that the peaks associated with the typical geopolymer structure, situated between 371 cm^{-1} and 712 cm^{-1}, remain unaltered. Conversely, vibrational peaks representing SO_4^{2-} (989 cm^{-1}) and calcite (1085 cm^{-1}) were observed to emerge, as previously discussed (as depicted in **Fig. 5**). When the geopolymer with in-situ ettringite was immersed in a solution, no significant alterations were observed as a function of the initial SeO_3^{2-} concentration. However, there was a noticeable weakening in the intensity of the peak

539 associated with SO_4^{2-} at 989 cm^{-1}, which may be attributed to the dissolution of potassium sulphate
540 present in the geopolymer with in-situ ettringite. Nevertheless, it was still possible to observe peaks
541 attributed to SO_4^{2-} vibrations in the geopolymer with in-situ ettringite that are considered to be derived
542 from the in-situ ettringite, and there was no significant change in these peaks. Unlike the synthetic
543 ettringite, it had no significant change of the broadband between 3000 cm^{-1} and 3650 cm^{-1}, especially the
544 peak representing O-H (around 3620 cm^{-1}), as a function of the initial concentration of SeO_3^{2-}.

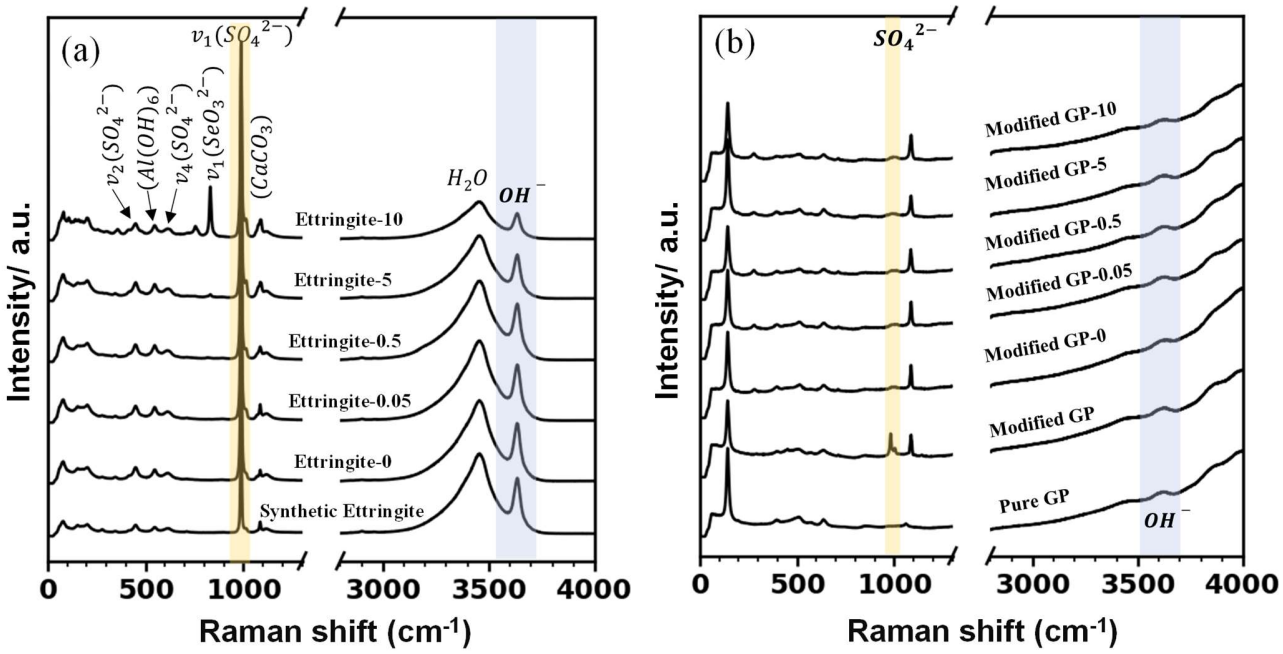

545

546 **Fig. 11.** Raman spectra of (a) synthetic ettringite and (b) geopolymer with in-situ ettringite after 14 days
547 of SeO_3^{2-} uptake at various initial concentrations (as marked in the dataset labels; values in mmol/L).
548 The vibration of each main functional group is marked in the figure by text annotations, and the vibrations
549 of OH^- and SO_4^{2-} are marked in the ribbons of light blue and light yellow, respectively.

550

551 In order to gain a deeper understanding of the alteration of -OH_2 groups in the synthetic ettringite
552 structure following the incorporation of SeO_3^{2-}, thermo gravimetric analysis (TG) was carried out. **Fig.**
553 **12** presents the TG profiles of synthetic ettringite after being immersed in various SeO_3^{2-} solutions. The

most substantial weight loss of the synthetic ettringite was observed between 90 and 108 ℃ and increased progressively with increasing temperature. The maximum weight loss was reached when the temperature rose to approximately 800 ℃, which can be attributed to the quantity of water present in the ettringite structure [68]. As the initial SeO_3^{2-} concentration increased, the water content in the ettringite structure after the uptake of SeO_3^{2-} decreased, with a notably significant reduction observed at an initial SeO_3^{2-} concentration of 10 mmol/L. The results are consistent with those obtained from the previous liquid phase analysis (represented in **Fig. 8** and **Fig. 9**) and provide evidence from the solid phase structure that the uptake of SeO_3^{2-} into ettringite through anion exchange at low SeO_3^{2-} concentrations does not alter the vibrational bond in the range of 3000 cm^{-1} to 3650 cm^{-1}. However, ligand exchange in the intercolumn edge site can reduce the amount of -OH_2 groups coordinated with Ca, which decreases the water content in synthetic ettringite and weakens the vibrational bond in the range of 3000 cm^{-1} to 3650 cm^{-1}.

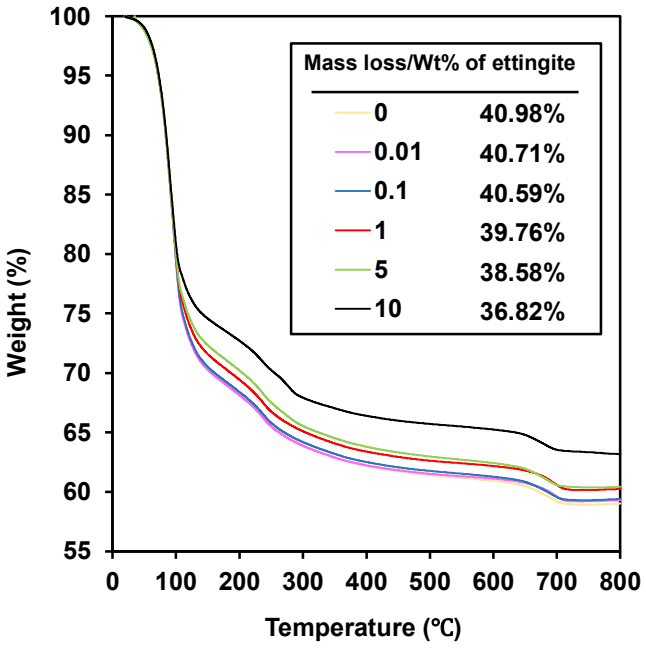

Fig. 12. TG curves of synthetic ettringite after immersion in various concentrations of SeO_3^{2-} solutions (as marked in the legend, in mmol/L) for 14 days

3.5 Thermodynamic modelling and verification

The ion exchange model was used to predict SeO_3^{2-} uptake at concentrations below 1 mmol/L, where uptake is primarily controlled via the ion exchange mechanism. The best fit of log_*K* was obtained through python-code fitting results with experimental data for SO_4^{2-} leaching (**Fig. 13 (a)** and **Fig. 13 (c)**). A high correlation between experimental data and modelling results was observed for both cases. The estimated log_*K* for ion exchange reaction in the synthetic ettringite and modified geopolymers are 1.049 and 0.222, respectively. The estimated log_*K* indicates that the ion exchange capacity of in-situ ettringite present in modified geopolymers is somewhat weakened by the geopolymer matrix, supporting the results shown in the previous sections. **Fig. 13 (b)** and **Fig. 13 (d)** depict the predicted amount of bound SeO_3^{2-} corresponding to estimated log_*K* as a function of concentration. The model prediction displays a good agreement with the experimental data, which describes and demonstrates the ion exchange mechanism at this concentration range.

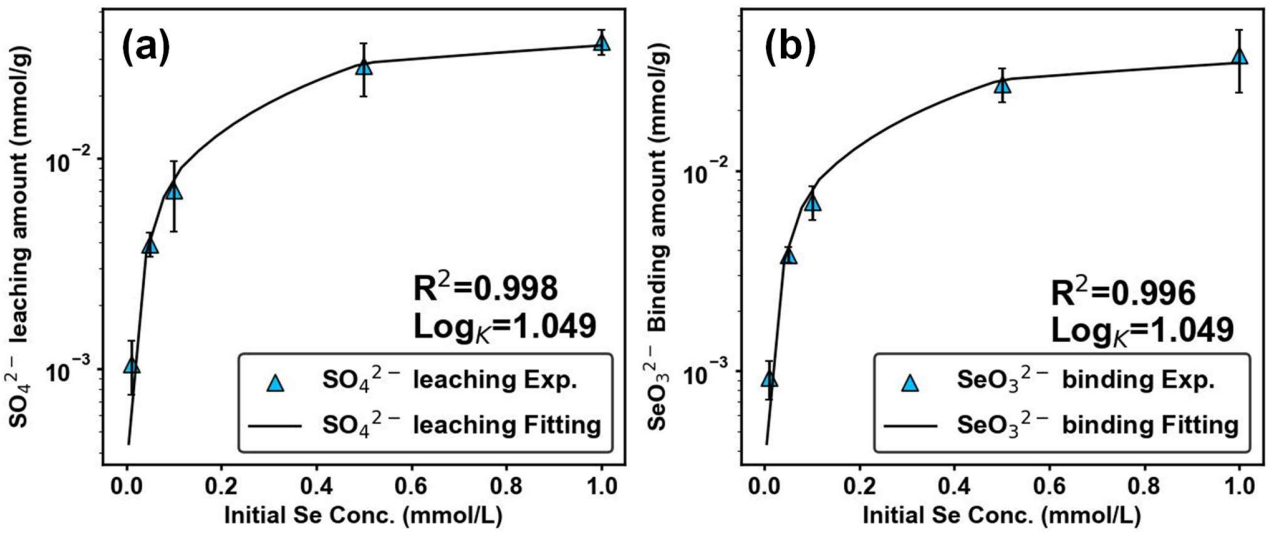

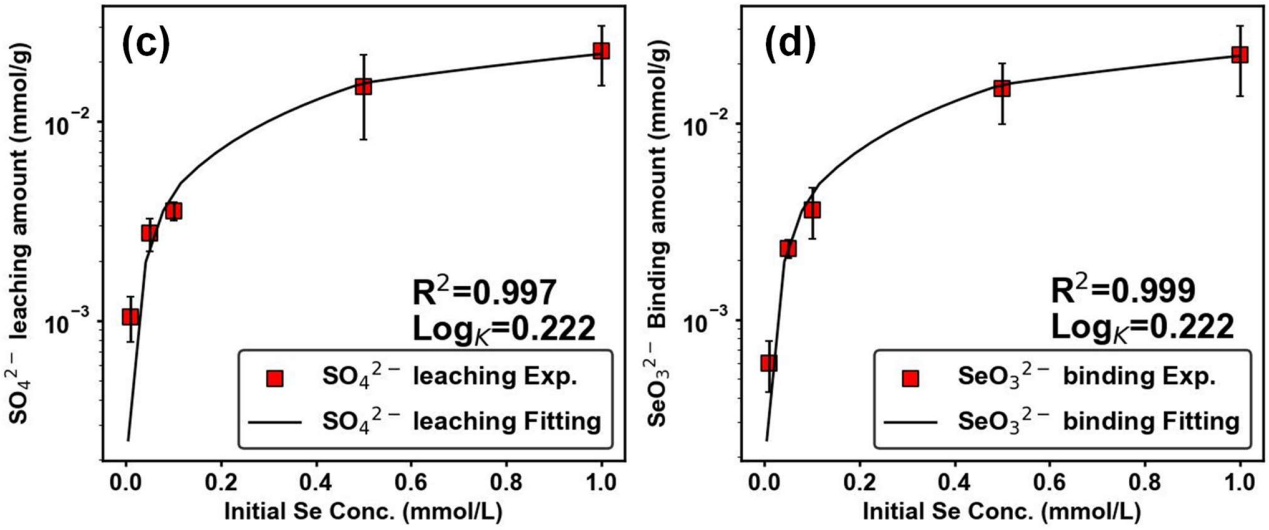

584

585 **Fig. 13.** Fitting of SO_4^{2-} leaching experimental data with modelling results for (a) synthetic ettringite
586 and (c) modified geopolymers, and the comparison of the predicted and measured uptake of SeO_3^{2-} for
587 (c) synthetic ettringite and (d) modified geopolymers as a function of concentration

588

589 **3.6 Mechanism of SeO_3^{2-} uptake in the geopolymer with in-situ ettringite**

590 The uptake mechanism of the geopolymer with in-situ ettringite for SeO_3^{2-} is schematically demonstrated
591 in **Fig. 14**. As discussed above, the mechanism for uptake of SeO_3^{2-} by ettringite strongly depends on the
592 concentration of SeO_3^{2-} in the solution. At low concentrations (< 1 mmol/L), the uptake of SeO_3^{2-} is
593 primarily dominated by ion exchange with inter-channels SO_4^{2-}. However, as the initial SeO_3^{2-}
594 concentration increases, ettringite immobilises SeO_3^{2-} through a ligand exchange with $-OH_2$ coordinated
595 with Ca located on the channel edges. According to the bond valence theory [42], the preferred structure
596 of complexes formed is shown in **Fig. 14**. The reason for such a mechanistic shift may be attributed to
597 the variation in the chemical potential generated by the concentrations of SeO_3^{2-} in solution [69]. When
598 the concentration of SeO_3^{2-} in a reaction system increases, the corresponding increase in its chemical
599 potential can facilitate its exchange with coordinated hydroxyl through a ligand exchange mechanism
600 [70]; this property of chemical potential is a critical factor that determines the selectivity and

601 controllability of chemical reactions involving ligand and ion exchange mechanisms. However, when
602 ettringite is present in its in-situ form in the geopolymer matrix, the positively charged embedded
603 ettringite could be attracted by the negatively charged geopolymer matrix by electrostatic forces. Due to
604 the polarity of the linked oxygen atoms, the proton in the channel edge functional group ($Ca\text{-}OH_2$) in the
605 ettringite structure may form hydrogen bonds with Al in the negatively charged tetrahedral AlO_4 on the
606 geopolymer surface, thus rendering these $-OH_2$ ligands somewhat more stable. At the same time, the
607 geopolymer matrix also covers most of the ettringite surface, physically obscuring to some degree the
608 sites on the ettringite surface where ligand exchange with SeO_3^{2-} can occur. Thus, the uptake capacity of
609 in-situ ettringite in modified geopolymer to SeO_3^{2-} through ligand exchange is sterically shielded by
610 geopolymer matrix to some extent; as a result, ion exchange with inter-channels SO_4^{2-} becomes the
611 controlling uptake mechanism of geopolymer with in-situ ettringite for SeO_3^{2-}. The ion exchange
612 capacities of ettringite and geopolymer for anions and cations, respectively, are influenced by each other
613 due to the compensation of mutually opposite charges. Nonetheless, it is noteworthy that the geopolymer
614 incorporating in-situ ettringite continues to exhibit a reasonable capacity for immobilising both cationic
615 and anionic radionuclides. These radionuclides are typically encountered in waste streams at
616 concentrations ranging from parts per million.

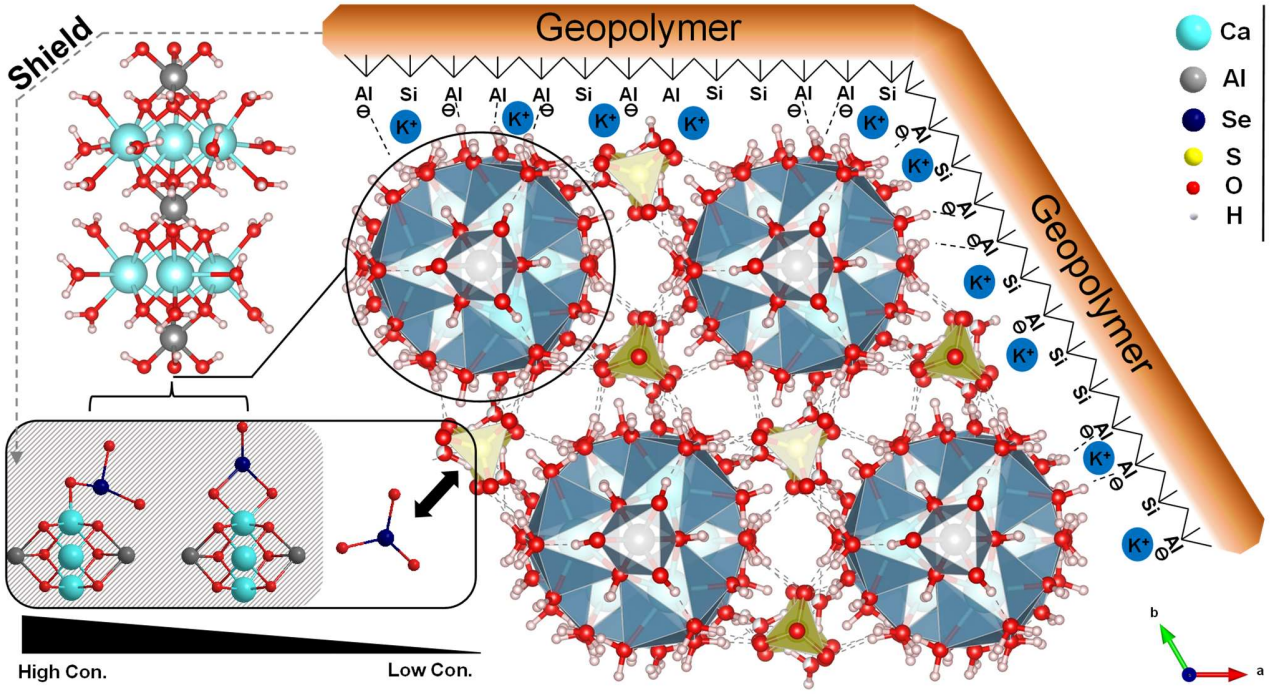

617

618 **Fig. 14.** A proposed mechanism for SeO_3^{2-} uptake in geopolymer with in-situ ettringite

619

620 **4. Conclusions**

621 Modified geopolymers with in-situ ettringite were successfully synthesised with the addition of gypsum
622 and ground granulated blast furnace slag (Gyp 10wt% + 3Slag). Ettringite was observed to have a high
623 uptake potential for Se oxyanions, and so its in situ synthesis endows geopolymer with a greatly enhanced
624 uptake capacity for Se oxyanions. Specific findings of this study include:

625 ➢ Either in the in-situ form or by co-precipitation, the generated ettringite can act in combination with
626 the permanently negatively charged geopolymer due to its positively charged surface, and this
627 interaction compensates for the partial negative charge.

628 ➢ The basic structure and cation uptake capacity of the geopolymer are retained after the modification
629 by ettringite synthesis.

630 ➢ Synthetic ettringite can immobilise both SeO_3^{2-} and SeO_4^{2-} through co-precipitation but can only
631 uptake SeO_3^{2-} through the binding process. The primary mechanism for immobilising SeO_3^{2-} during

632 the binding process is through ion exchange with SO_4^{2-} at low concentrations (<1 mmol/L). The
633 maximum ion exchange capacity at around 1 mmol/L is approximately 0.037 mmol/g. However, at
634 higher concentrations (>1 mmol/L), the dominant mechanism shifts to ligand exchange with Ca-OH_2.
635 A maximum R_d value of approximately 0.092 was obtained in the concentrations of 0.01, 5, and 10
636 mmol/L.

637 ➢ The uptake mechanism of ligand exchange to SeO_3^{2-} is partially shielded by the electrostatic
638 interaction and hydrogen bonding with the geopolymer matrix. However, the modified geopolymer
639 retains the capacity to adsorb cationic radionuclides (Cs^+ and Sr^{2+}) and has developed significant
640 uptake capacity for SeO_3^{2-} by ion exchange as the controlling mechanism. The maximum
641 immobilisation capacities for Cs^+, Sr^{2+} and SeO_3^{2-} were approximately 0.597, 0.974 and 0.096
642 mmol/g, respectively.

643 ➢ Thermodynamic modelling was conducted based on an ion exchange mechanism, which predicts the
644 uptake behaviour of both synthetic ettringite and modified geopolymers for SeO_3^{2-} at low
645 concentrations (< 1 mmol/L).

646

647 **CRediT authorship contribution statement**

648 **Xiaobo Niu:** Conceptualisation, Methodology, Formal analysis, Validation, Writing-original Draft,
649 Investigation, Data Curation, Writing-review & editing.

650 **Yogarajah Elakneswaran:** Conceptualisation, Methodology, Formal analysis, Writing-original Draft,
651 Supervision, Writing-review & editing.

652 **Chaerun Raudhatul Islam:** Methodology, Investigation, Data Curation, Writing-review & editing.

653 **Chuwei Fang:** Methodology, Investigation, Data Curation, Writing-review & editing.

654 **Naoki Hiroyoshi:** Conceptualisation, Supervision, Writing-review & editing, Project administration.

John L. Provis: Conceptualisation, Funding acquisition, Supervision, Writing-review & editing, Project administration.

Tsutomu Sato: Conceptualisation, Funding acquisition, Supervision, Writing-review & editing, Project administration.

Declaration of Competing Interest

The authors declare that they have no known competing financial interests or personal relationships that could have appeared to influence the work reported in this paper.

Acknowledgements

JAEA Nuclear Energy S&T and Human Resource Development Project supported part of this work through concentrating wisdom Grant Number JPJA20P12345678 and EPSRC (UK) under grants EP/T013524/1. A part of this work was supported by JST SPRING, Grant Number JPMJSP2119.

References

[1] J.E.Spallholz, On the nature of selenium toxicity and carcinostatic activity, Free Radic. Biol. Med., 17(1994) 45-64. http://doi.org/10.1016/0891-5849(94)90007-8

[2] TEPCO, Basic Policy for the Contaminated Water Issue at the TEPCO's Fukushima Daiichi Nuclear Power Station, (2013). https://www.mofa.go.jp/policy/page3e_000072.html

[3] G. Jörg, R. Bühnemann, S. Hollas, N. Kivel, K. Kossert, S. V. Winckel, C. L. v. Gostomski, Preparation of radiochemically pure ^{79}Se and highly precise determination of its half-life, Appl. Radiat. Isot., 68(2010) 2339-2351. https://doi.org/10.1016/j.apradiso.2010.05.006.

677 [4] H. Sekimoto, H. Nakamura, N. Takagi, Toxicity of radioactive wastes discharged from nuclear energy
678 centre in the future equilibrium state, Ann. Nucl. Energy, 23(1996) 663-668.
679 https://doi.org/10.1016/0306-4549(95)00031-3.
680 [5] S. O. Okonji, L. Yu, J. A. Dominic, D. Pernitsky, G. Achari, Adsorption by Granular Activated
681 Carbon and Nano Zerovalent Iron from Wastewater: A Study on Removal of Selenomethionine and
682 Selenocysteine, Water, 13(2021) 23. https://doi.org/10.3390/w13010023
683 [6] X. Zhang, X. Li, Z. Jin, S. H. Tumrani, X. Ji, Selenium in wastewater can be adsorbed by modified
684 natural zeolite and reused in vegetable growth, Sci. Prog., 104(2021) 1-20.
685 https://doi.org/10.1177/00368504211019845.
686 [7] T. Nishimura, H. Hashimoto, M. Nakayama, Removal of Selenium(VI) from Aqueous Solution with
687 Polyamine - type Weakly Basic Ion Exchange Resin, Sep. Purif. Technol., 42(2007) 3155-3167.
688 https://doi.org/10.1080/01496390701513107.
689 [8] S. O. Okonji, J. A. Dominic, D. Pernitsky, G. Achari, Removal and recovery of selenium species
690 from wastewater: Adsorption kinetics and co-precipitation mechanisms, J. Water Process. Eng., 38(2020)
691 101666. https://doi.org/10.1016/j.jwpe.2020.101666.
692 [9] TEPCO, n.d. Contaminated Water Treatment. (2023).
693 https://www.tepco.co.jp/en/decommision/planaction/alps/index-e.html
694 [10] M. H. Zeeshan, R. U. Khan, M. Shafiq, A. Sabir, Polyamide intercalated nanofiltration membrane
695 modified with biofunctionalised core shell composite for efficient removal of Arsenic and Selenium from
696 wastewater, J. Water Process. Eng., 34(2020) 101175. https://doi.org/10.1016/j.jwpe.2020.101175.
697 [11] H. K. Hansen, S. F. Peña, C. Gutiérrez, A. Lazo, P. Lazo, L. M. Ottosen, Selenium removal from
698 petroleum refinery wastewater using an electrocoagulation technique, J. Hazard. Mater., 364(2019) 78-
699 81. https://doi.org/10.1016/j.jhazmat.2018.09.090.

[12] E. Lichtfouse, N. M. Crini, C. Bradu, Y. A. Boussouga, M. Aliaskari, A. I. Schäfer, S. Das, L. D. Wilson, M. Ike, D. Inoue, M. Kuroda, S. Déon, P. Fievet, G. Crini, Technologies to Remove Selenium from Water and Wastewater, Emerg. Contam. Vol. 2., 2(2021) 207-304. https://doi.org/10.1007/978-3-030-69090-8_3.

[13] L. Zhu, L. Zhang, J. Li, D. Zhang, L. Chen, D.. Sheng, S. Yang, C. Xiao, J. Wang, Z. Chai, T. E. Albrecht-Schmitt, S. Wang, Selenium Sequestration in a Cationic Layered Rare Earth Hydroxide: A Combined Batch Experiments and EXAFS Investigation, Environ. Sci. Technol., 51(2017) 8606–8615. https://doi.org/10.1021/acs.est.7b02006

[14] J. Li, B. Li, N. Shen, L. Chen, Q. Guo, L. Chen, L. He, X. Dai, Z. Chai, S. Wang, Task-Specific Tailored Cationic Polymeric Network with High Base-Resistance for Unprecedented 99TcO4– Cleanup from Alkaline Nuclear Waste, ACS Cent. Sci., 7(2021) 1441–1450. https://doi.org/10.1021/acscentsci.1c00847

[15] L. Zhu, D. Sheng, C. Xu, X. Dai, M. A. Silver, J. Li, P. Li, Y. Wang, Y. Wang, L.. Chen, C. Xiao, J.. Chen, R. Zhou, C. Zhang, O. K. Farha, Z. Chai, T. E. Albrecht-Schmitt, S. Wang, Identifying the Recognition Site for Selective Trapping of $^{99}TcO_4^-$ in a Hydrolytically Stable and Radiation Resistant Cationic Metal–Organic Framework, J. Am. Chem. Soc., 139(2017) 14873–14876. https://doi.org/10.1021/jacs.7b08632

[16] N. Shen, Z. Yang, S. Liu, X. Dai, C. Xiao, K. Taylor-Pashow, D. Li, C. Yang, J. Li, Y. Zhang, M. Zhang, R. Zhou, Z. Chai, S. Wang, $^{99}TcO_4^-$ removal from legacy defense nuclear waste by an alkaline-stable 2D cationic metal organic framework, Nat. Commun., 11(2020) 5571. https://doi.org/10.1038/s41467-020-19374-9

[17] X. Zhang, Y. Guo, N. Xie, R. Guo, Y. Wang, Z. Hu, W. Xu, Y. Ai, J. Gao, J. Wang, Q. Liang, D. Niu, H. Sun, Y. Qi, Ternary NiFeMnOx compounds for adsorption of antimony and subsequent application in energy storage to avoid secondary pollution, Sep. Purif. Technol., 276(2021) 119237. https://doi.org/10.1016/j.seppur.2021.119237.

725 [18] J.L. Provis, Geopolymers and other alkali activated materials - Why, how, and what?, Mater. Struct.,
726 47(2014) 11-25. https://doi.org/10.1617/s11527-013-0211-5
727 [19] J. L. Provis and S. A. Bernal, Geopolymers and related alkali-activated materials, Annu. Rev. Mater.
728 Sci., 44(2014) 299-327. https://doi.org/10.1146/annurev-matsci-070813-113515
729 [20] V. Cantarel, T. Motooka, I. Yamagishi, Geopolymers and their potential applications in the nuclear
730 waste management field A bibliographical study, (2017)014. Japan https://doi.org/10.11484/jaea-review-
731 2017-014
732 [21] Y. Huang, M. Han, The influence of α-Al_2O_3 addition on microstructure, mechanical and
733 formaldehyde adsorption properties of fly ash-based geopolymer products, J. Hazard. Mater., 193(2011)
734 90–94. https://doi.org/10.1016/j.jhazmat.2011.07.029
735 [22] Q. Li, Z. Sun, D. Tao, Y. Xu, P. Li, H. Cui, J. Zhai, Immobilisation of simulated radionuclide $^{133}Cs^{+}$
736 by fly ash-based geopolymer. J. Hazard. Mater., 262(2013) 325–331.
737 https://doi.org/10.1016/j.jhazmat.2013.08.049
738 [23] P. He, J. Cui, M. Wang, S. Fu, H. Yang, C. Sun, X. Duan, Z. Yang, D. Jia, Y. Zhou, Interplay
739 between storage temperature, medium and leaching kinetics of hazardous wastes in metakaolin-based
740 geopolymer, J. Hazard. Mater., 384(2020) 121377 https://doi.org/10.1016/j.jhazmat.2019.121377
741 [24] D. A. Geddes, X. Ke, S. A. Bernal, M. Hayes, J. L. Provis, Metakaolin-Based Geopolymers for
742 Nuclear Waste Encapsulation. In: Martirena, F., Favier, A., Scrivener, K. (eds) Calcined Clays for
743 Sustainable Concrete, RILEM Bookseries, Springer, Dordrecht, 16(2018). https://doi.org/10.1007/978-
744 94-024-1207-9_29
745 [25] INTERNATIONAL ATOMIC ENERGY AGENCY, Combined Methods for Liquid Radioactive
746 Waste Treatment, IAEA-TECDOC-1336, IAEA, Vienna (2003).
747 [26] S. A. Bernal, J. S. J. van Deventer, J. L. Provis, What happens to 5-year-old metakaolin
748 geopolymers? The effect of alkali cation. In: Scrivener, K., Favier, A. (eds) Calcined Clays for

749 Sustainable Concrete. RILEM Bookseries, Springer, Dordrecht, 10(2015). https://doi.org/10.1007/978-
750 94-017-9939-3_39
751 [27] A. Palomo, A. Fernández-Jiménez, M. Criado, Geopolymers: same basic chemistry, different
752 microstructures, Mater. Constr., 54(275) (2004) 77–91. https://doi.org/10.3989/mc.2004.v54.i275.249
753 [28] A. A. Siyal, M. R. Shamsuddin, M. I. Khan, N. E. Rabat, M. Zulfiqar, Z. Man, J. Siame, K. A. Azizli,
754 A review on geopolymers as emerging materials for the adsorption of heavy metals and dyes. J. Environ.
755 Manage., 224(2018) 324-339. https://doi.org/10.1016/j.jenvman.2018.07.046
756 [29] F. J. López, S. Sugita, M. Tagaya, T. Kobayashi, Metakaolin-Based Geopolymers for Targeted
757 Adsorbents to Heavy Metal Ion Separation. J. Mater. Sci. Chem. Eng., 02(2014) 16–27.
758 https://doi.org/10.4236/MSCE.2014.27002
759 [30] N. Soonthornwiphat, Y. Kobayashi, K. Toda, K. Kuroda, C. R. Islam, T. Otake, Y. Elakneswaran,
760 J. L. Provis, T. Sato, Encapsulation of Sr-loaded titanate spent adsorbents in potassium aluminosilicate
761 geopolymer, J. Nucl. Sci. Technol., 19(2020) 1181-1188.
762 https://doi.org/10.1080/00223131.2020.1775717
763 [31] Q. Tian and K. Sasaki, Application of fly ash-based geopolymer for removal of caesium, strontium
764 and arsenate from aqueous solutions: Kinetic, equilibrium and mechanism analysis. Water Sci. Technol.,
765 79(2019) 21162125. https://doi.org/10.2166/wst.2019.209
766 [32] N. Vandevenne, R. I. Iacobescu, Y. Pontikes, R. Carleer, E. Thijssen, K. Gijbels, S. Schreurs, W.
767 Schroeyers, Incorporating Cs and Sr into blast furnace slag inorganic polymers and their effect on matrix
768 properties. J. Nucl. Mater., 503(2018) 1–12. https://doi.org/10.1016/J.JNUCMAT.2018.02.023
769 [33] X. Niu, Y. Elakneswaran, R. I. Chaerun, J. L. Provis, T. Sato, Adsorption behaviour of simulant
770 radionuclide cations and anions in metakaolin-based geopolymer, J. Hazard. Mater., 429(2022) 128373.
771 https://doi.org/10.1016/j.jhazmat.2022.128373
772 [34] H.F.W. Taylor, Cement Chemistry, 2nd edition, Academic Press Limited, New York (1997).
773 https://www.icevirtuallibrary.com/doi/pdf/10.1680/cc.25929.fm

774 [35] A.E. Moore, H.F.W. Taylor, Crystal structure of ettringite, Acta Crystallogr., B26(1970) 386-393.
775 https://doi.org/10.1107/S0567740870002443
776 [36] H.F.W. Taylor, Crystal structures of some double hydroxide minerals. Mineralogical Magazine,
777 39(1973) 377-389. https://doi:10.1180/minmag.1973.039.304.01
778 [37] N. Saikia, S. Kato, T. Kojima, Behavior of B, Cr, Se, As, Pb, Cd, and Mo present in waste leachates
779 generated from combustion residues during the formation of ettringite, Environ. Toxicol. Chem.,
780 25(2006) 1710-1719. https://doi.org/10.1897/05-625R.1
781 [38] M. Chrysochoou, D. Dermatas, Evaluation of ettringite and hydrocalumite formation for heavy
782 metal immobilisation: Literature review and experimental study, J. Hazard. Mater., 136(2006) 20-33.
783 https://doi.org/10.1016/j.jhazmat.2005.11.008.
784 [39] J.K. Solem-Tishmack, G.J. McCarthy, B. Docktor, K.E. Eylands, J.S. Thompson, D.J. Hassett,
785 High-calcium coal combustion by-products: Engineering properties, ettringite formation, and potential
786 application in solidification and stabilisation of selenium and boron, Cem Concr Res., 25 (1995) 658-
787 670. https://doi.org/10.1016/0008-8846(95)00054-G.
788 [40] M. Zhang and E. J. Reardon, Removal of B, Cr, Mo, and Se from Wastewater by Incorporation into
789 Hydrocalumite and Ettringite, Environ. Sci. Technol., 37(2007) 2947-2952.
790 https://doi.org/10.1021/es020969i
791 [41] B. Guo, K. Sasaki, T. Hirajima, Characterisation of the intermediate information of selenate-
792 substituted ettringite, Cem. Concr. Res., 99(2017) 30-37.
793 https://doi.org/10.1016/j.cemconres.2017.05.002.
794 [42] B. Guo, K. Sasaki, T. Hirajima, Selenite and selenate uptaken in ettringite: Immobilisation
795 mechanisms, coordination chemistry, and insights from structure, Cem. Concr. Res., 100(2017) 166-175.
796 https://doi.org/10.1016/j.cemconres.2017.07.004.
797 [43] S. Wang, K. L. Scrivener, Hydration products of alkali-activated slag cement, Cem. Concr. Res.,
798 25(1995) 561-571, https://doi.org/10.1016/0008-8846(95)00045-E.

799 [44] C. Li, H. Sun, L. Li, A review: The comparison between alkali-activated slag (Si+Ca) and
800 metakaolin (Si+Al) cements, Cem. Concr. Res., 40(2010) 1341-1349,
801 https://doi.org/10.1016/j.cemconres.2010.03.020.
802 [45] A. Palomo, M. Palacios, Alkali-activated cementitious materials: Alternative matrices for the
803 immobilisation of hazardous wastes: Part II. Stabilisation of chromium and lead, Cem. Concr. Res.,
804 33(2003) 289-295. https://doi.org/10.1016/S0008-8846(02)00964-X.
805 [46] P. Chindaprasirt, S. Thaiwitcharoen, S. Kaewpirom, U. Rattanasak, Controlling ettringite formation
806 in FBC fly ash geopolymer concrete, Cem. Concr. Compos., 41(2013) 24-28.
807 https://doi.org/10.1016/j.cemconcomp.2013.04.009.
808 [47] P. Sukmak, P. De. Silva, S. Horpibulsuk, P. Chindaprasirt, Sulphate Resistance of Clay-Portland
809 Cement and Clay High-Calcium Fly Ash Geopolymer, J. Mater. Civ. Eng., 27(2015) 5.
810 https://doi.org/10.1061/(ASCE)MT.1943-5533.0001112.
811 [48] S. Chen, Y. Qi, J. J. Cossa, I. D. S. Dos Santos, Efficient removal of radioactive iodide anions from
812 simulated wastewater by HDTMA-geopolymer, Prog. Nucl. Energy, 177(2019) 103112.
813 https://doi.org/10.1016/j.pnucene.2019.103112.
814 [49] Z. Ji, Y. Pei, Immobilisation efficiency and mechanism of metal cations (Cd^{2+}, Pb^{2+} and Zn^{2+}) and
815 anions (AsO_4^{3-} and $Cr_2O_7^{2-}$) in wastes-based geopolymer, J. Hazard. Mater., 384(2020) 121290.
816 https://doi.org/10.1016/j.jhazmat.2019.121290.
817 [50] Q. Tian, K. Sasaki, A novel composite of layered double hydroxide/geopolymer for co-
818 immobilisation of Cs^+ and SeO_4^{2-} from aqueous solution, Sci. Total. Environ., 695(2019) 133799.
819 https://doi.org/10.1016/j.scitotenv.2019.133799.
820 [51] P. Ježek, P. Škarpa, T. Lošák, J. Hlušek, M. Jůzl and P. Elzner, Selenium – An Important Antioxidant
821 in Crops Biofortification, Antioxidant Enzyme. InTech., (2012) 343-368. https://dx.
822 doi.org/10.5772/50356

[52] D.L. Parkhurst, C.A.J. Appelo, User's Guide to PHREEQC (Version 2)—A Computer Program for Speciation, Batch-Reaction, One-Dimensional Transport, and Inverse Geochemical Calculations. U.S. Geological Survey, Water Resources Investigations Report (1999) 99-4259, Washington DC. https://doi.org/10.3133/wri994259

[53] C.A.J. Appelo, D.L. Parkhurst, Description of input and examples for PHREEQC version 3—a computer program for speciation, batch-reaction, one-dimensional transport, and inverse geochemical calculations. US geological survey techniques and methods, 6.A43(2013) 497.

[54] L. Divet, R. Randriambololona, Delayed Ettringite Formation: The Effect of Temperature and Basicity on the Interaction of Sulphate and C-S-H Phase, Cem. Concr. Res., 28(1998) 357-363. https://doi.org/10.1016/S0008-8846(98)00006-4.

[55] R. B. Jewell, R. Rathbone, T. Duvallet, T. L. Robl, Kamyar C. Mahboub, Fabrication and Testing of Low-Energy Calcium Sulfoaluminate-Belite Cements that Utilise Fluidised Bed Combustion By-Products, Coal Combust. Gasific. Prod., 7(2015) 9-18. https://doi.org/10.4177/CCGP-D-15-00001.1

[56] G. Renaudin, R. Segni, D. Mentel, J. M. Nedelec, F. Leroux, C. T. Gueho, A Raman Study of the Sulphated Cement Hydrates: Ettringite and Monosulfoaluminate, J. Adv. Concr. Technol., 5(2007) 299-312. https://doi.org/10.3151/jact.5.299

[57] R. I. Chaerun, N. Soonthornwiphat, K. Toda, K. Kuroda, X. Niu, R. Kikuchi, T. Otake, Y. Elakneswaran, J. L. Provis, T. Sato, Retention Mechanism of Cesium in Chabazite Embedded into Metakaolin-Based Alkali Activated Materials, J. Hazard. Mater., 440(2022) 129732. https://doi.org/10.1016/j.jhazmat.2022.129732.

[58] P.P. Knops-Gerrits, D.E. De Vos, E.J.P. Feijen, P.A. Jacobs, Raman spectroscopy on zeolites, Microporous Mater., 8 (1997) 3-17. https://10.1016/S0927-6513(96)00088-0.

[59] J.K. Solem-Tishmack, G.J. McCarthy, B. Docktor, K.E. Eylands, J.S. Thompson, D.J. Hassett, High-calcium coal combustion by-products: Engineering properties, ettringite formation, and potential

847 application in solidification and stabilisation of selenium and boron, Cem. Concr. Res., 25(1995) 658-
848 670. https://doi.org/10.1016/0008-8846(95)00054-G.
849 [60] M. R. Hartman, S. K. Brady, R. Berliner, M. S. Conradi, The evolution of structural changes in
850 ettringite during thermal decomposition, J. Solid State Chem., 179(2006) 1259-1272.
851 https://doi.org/10.1016/j.jssc.2006.01.038.
852 [61] L. Eklund, I. Persson, Structure and hydrogen bonding of the hydrated selenite and selenate ions in
853 aqueous solution, Dalton Trans. 43(2014) 6315-21. https://doi.org/10.1039/C3DT53468E.
854 [62] S. Sharmasarkar, G. F Vance, Selenite–selenate sorption in surface coal mine environment, Adv.
855 Ecol. Res., 7(2002) 87-95. https://doi.org/10.1016/S1093-0191(01)00110-1.
856 [63] B. Guo, Q. Tian, T. Oji, L. Wang, K. Sasaki, Effects of Mg compounds in hydroxylated calcined
857 dolomite as an effective and sustainable substitute of lime to precipitate as ettringite for treatment of
858 selenite/selenate in aqueous solution, Colloids Surf. A Physicochem. Eng. Asp., 610(2021) 125782,
859 https://doi.org/10.1016/j.colsurfa.2020.125782.
860 [64] M.R. Hartman, R. Berliner, Investigation of the structure of ettringite by time-of-flight neutron
861 powder diffraction techniques, Cem. Concr. Res., 36(2006) 364-370.
862 https://doi.org/10.1016/j.cemconres.2005.08.004.
863 [65] G. D. Gatta, U. Hålenius, F. Bosi, L. C. Delgado, M. T. F. Diaz; Minerals in cement chemistry: A
864 single-crystal neutron diffraction study of ettringite, $Ca_6Al_2(SO_4)_3(OH)_{12}\cdot 27H_2O$. American
865 Mineralogist, 104(2019) 73–78. https://doi.org/10.2138/am-2019-6783
866 [66] Goetz-Neunhoeffer, F., & Neubauer, J, Refined ettringite ($Ca_6Al_2(SO_4)_3(OH)_{12}\cdot 26H_2O$) structure
867 for quantitative X-ray diffraction analysis. Powder Diffraction, 21(2006) 4-11.
868 https://doi:10.1154/1.2146207
869 [67] I. Baur and C. A. Johnson, Sorption of Selenite and Selenate to Cement Minerals, Environ. Sci.
870 Technol., 37(2003) 3442-3447. https://doi.org/10.1021/es020148d

871 [68] R. B. Perkins, C. Palmer, Solubility of ettringite ($Ca_6[Al(OH)_6]_2(SO_4)_3 \cdot 26H_2O$) at 5–75°C, Geochim.
872 Cosmochim Acta, 63(1999) 1969-1980. https://doi.org/10.1016/S0016-7037(99)00078-2.
873 [69] Bootharaju, M. Siddaramappa, Reversible Size Control of Silver Nanoclusters via Ligand-Exchange,
874 Chem. Mater., 27(2015) 4289-4297. https://doi.org/10.1021/acs.chemmater.5b00650
875 [70] G. H. Woehrle, L. O. Brown, J. E. Hutchison, Thiol-Functionalised, 1.5-nm Gold Nanoparticles
876 through Ligand Exchange Reactions: Scope and Mechanism of Ligand Exchange, J. Am. Chem. Soc.,
877 127(2005) 2172–2183. https://doi.org/10.1021/ja0457718
878 [71] N. Takeno, Atlas of Eh-pH diagrams - Intercomparison of thermodynamic databases, Open File
879 Report of GSJ, 419(2005). Geological Survey of Japan, AIST.
880
881
882
883
884
885
886

Supporting Information

1. Thermodynamic ion exchange model and its fitting method

Python-written best Log_k fitting code template

The following Python-IPhreeqcCOM template code simplifies the search for the best fitting $\boldsymbol{Log_k}$ values between the results obtained from Phreeqc and experimental data. The search is automated using the least squares method, which gradually narrows down the range of values based on the parameters provided.

Initially, the experimental data is imported into the process, and the $\boldsymbol{Log_k}$ value is determined based on the provided boundary conditions. Next, the phreeqc module is utilised to calculate the leaching of SO_4^{2-}. A range of Se initial concentration-SO_4^{2-} leaching curves corresponding to different $\boldsymbol{Log_k}$ values is obtained, and the closeness of these curves to the experimental data is evaluated using the Root Mean Squared Error (RMSE). The least squares method is then applied to determine the best-fitting $\boldsymbol{Log_k}$ value within the given range, which corresponds to the smallest RMSE.

The code:

```
from win32com.client import Dispatch
import pandas as pd
import numpy as np
from scipy.stats import pearsonr
import matplotlib.pyplot as plt

# Creating PHREEQC objects
def GetResult(input_string, db_path = 'WATEQ4F.DAT'):
        dbase = Dispatch('IPhreeqcCOM.Object')
```

```
        dbase.LoadDatabase(db_path)
        dbase.RunString(input_string)
        output = dbase.GetSelectedOutputArray()
        return output

# Calculate the RMSE between two arrays
def calculate_rmse(a, b):
       return np.sqrt(np.mean((a - b)**2))

# Create a function that compares two sets of data
def calculate_correlation(a, b):
    corr, _ = pearsonr(a, b)
    return corr

# Calculate RMSE from log_k
def get_fit(K_fitting, Con, SO4_leaching_ex, SeO3_binding_ex):
                                    # Make sure experimental data has been imported
       SeO3_binding_f=[]
       SO4_leaching_f=[]
       for Se_con in Con:
              input_str = f'''
                     Phase
                            Ettringite    # In order to simulate the pH change and
                                          #SO42- environment in the experiment
                                   Ca6Al2(SO4)3(OH)12:26H2O + 12H+ = 2Al+++ + 6Ca++ + 38H2O +
3SO4--
                                   log_k 57.730
                                   delta_h -389.36
                     SOLUTION 1
                            units  mmol/kgw
                            Temp   20
                            ph     7      charge
                            water   1
                            Se(4) {Se_con}
                     EQUILIBRIUM_PHASES 1
                            Ettringite 0 0.000797 #Indicates the amount of
                            Save solution 1       #ettringite in the system at 1
```

```
951                 End                     #mol/L
952           EXCHANGE_MASTER_SPECIES
953                 Xg Xg+2
954
955           EXCHANGE_SPECIES
956                 Xg+2 = Xg+2
957                 log_k = 0
958
959                 Xg+2 + SO4-2 = XgSO4
960                 log_k = 0
961
962                 XgSO4 + SeO3-2 = XgSeO3 + SO4-2
963                 -gamma 3.5 0.015
964                 log_k = {K_fitting}
965
966           USE SOLUTION 1
967           EXCHANGE 1
968                 XgSO4 4e-5     #ettringite contains 0.004 mol/kg of
969           CALCULATE_VALUES      #exchangeable SO42-
970           SeO3(binding)
971           -start
972           10 m_Se = MOL("XgSeO3") *1000
973           100 SAVE m_Se
974           -end
975           SO4(leaching)
976           -start
977           10 m_S = (4e-5-MOL("XgSO4")) *1000
978           100 SAVE m_S
979           -end
980
981           SELECTED_OUTPUT
982           -reset false
983           -calculate_values SeO3(binding)
984           -calculate_values SO4(leaching)
985
986     '''
```

```
                output = GetResult(input_str)
                XgSeO3, SO4 = output[1]
                SeO3_binding_f.append(XgSeO3)
                SO4_leaching_f.append(SO4)

        fit = calculate_rmse(SO4_leaching_ex, SO4_leaching_f)
        return fit

#setting parameters  #Arbitrary starting conditions and boundaries can be set
min_fit = 1
K_fitting=0
best_fit=0
left = 0
right = 20
epsilon = 0.0001

# Loop calculation of fit
while right - left > epsilon:
    mid = (left + right) / 2
    fit = get_fit(mid)
    if fit < min_fit:
        min_fit = fit
        K_fitting = mid
    if fit < get_fit(mid+epsilon):
        right = mid
    else:
        left = mid

best_K_fitting = K_fitting
best_fit = get_fit(best_K_fitting)

plt.plot(x, y)
```

2. SeO_3^{2-} redox state

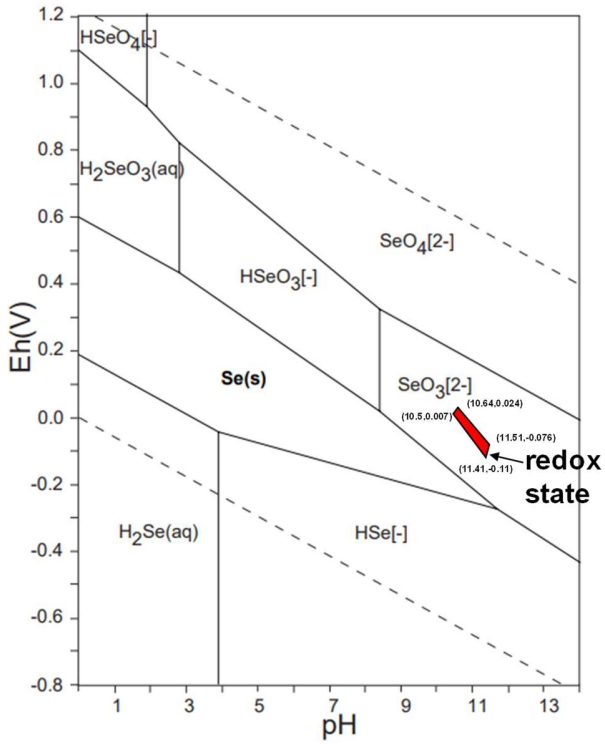

Fig. S1. Eh-pH diagram at 298.15 K, 10^5 Pa [71]. The redox state of SeO_3^{2-} in this study is marked in the red area.